JB Accepted Manuscript Posted Online 12 October 2015
J. Bacteriol. doi:10.1128/JB.00343-15
Copyright © 2015, American Society for Microbiology. All Rights Reserved.

Accepted Manuscript Posted Online
Journal of Bacteriology
JB
Journal of Bacteriology

Structural, functional and immunogenic insights on Cu,Zn Superoxide Dismutase pathogenic virulence factors from *Neisseria meningitidis* and *Brucella abortus*

Ashley J. Pratt[a,b*], Michael DiDonato[a*], David S. Shin[a,b], Diane E. Cabelli[c], Cami K. Bruns[a], Carol A. Belzer[d*], Andrew R. Gorringe[e], Paul R. Langford[f], Louisa B. Tabatabai[d*], J. Simon Kroll[f], John A. Tainer[b,g] and Elizabeth D. Getzoff[a#]

Department of Integrative Structural and Computational Biology and The Skaggs Institute for Chemical Biology, The Scripps Research Institute, La Jolla, CA, USA[a]; Life Sciences Division, Lawrence Berkeley National Laboratory, Berkeley, CA USA[b]; Chemistry Department, Brookhaven National Laboratory, Upton, NY, USA[c]; National Animal Disease Center, Ruminant Diseases and Immunology, Ames, IA, USA[d]; Public Health England (previously The Health Protection Agency), Porton Down, Salisbury, UK[e]; Section of Paediatrics, Department of Medicine, Imperial College London, St. Mary's Campus, London, England, UK[f]; Department of Molecular and Cellular Oncology, The University of Texas M.D. Anderson Cancer Center, Houston, TX, USA[g]

Running Head: *N. meningitidis* and *B. abortus* Cu,ZnSODs

#Address correspondence to Elizabeth D. Getzoff, edg@scripps.edu

*Present address: Ashley J. Pratt, Health Interactions, San Francisco, CA, USA; Michael DiDonato, Genomics Institute of the Novartis Research Foundation, San Diego, CA, USA; Carol

Accepted Manuscript Posted Online

A. Belzer, Center for Veterinary Biologics-Policy, Evaluation and Licensing, Biotechnology, Immunology and Diagnostics, Ames, IA, USA; Louisa B. Tabatabai, Roy J. Carver Dept. of Biochemistry, Biophysics & Molecular Biology, Iowa State University, Ames, IA, USA.

A.J.P. and M.D. contributed equally to this work.

ABSTRACT. Bacterial pathogens *Neisseria meningitidis* and *Brucella abortus* pose threats to human and animal health worldwide, causing meningococcal disease and brucellosis, respectively. Mortality from acute *N. meningitidis* infections remains high despite antibiotics, and brucellosis presents alimentary and health consequences. Superoxide dismutases are master regulators of reactive oxygen, general pathogenicity factors and therefore therapeutic targets. Cu,Zn superoxide dismutases (SODs) localized to the periplasm promote survival by detoxifying superoxide radicals generated by major host antimicrobial immune responses. We discovered that passive immunization with an antibody directed at *N. meningitidis* SOD (NmSOD) was protective in a mouse infection model. To define the relevant atomic details and solution assembly states of this important virulence factor, we report high-resolution and X-ray scattering analyses of NmSOD and SOD from *B. abortus* (BaSOD). The NmSOD structures revealed an auxiliary tetrahedral Cu-binding site bridging the dimer interface; mutational analyses suggested that this metal site contributes to protein stability, with implications for bacterial defense mechanisms. Biochemical and structural analyses informed us about electrostatic substrate guidance, dimer assembly and an exposed C-terminal epitope in the NmSOD dimer. In contrast, the monomeric BaSOD structure provided insights for extending immunogenic peptide epitopes derived from the protein. These collective results reveal unique contributions of SOD to

Journal of Bacteriology JB Journal of Bacteriology

Accepted Manuscript Posted Online

pathogenic virulence, refine predictive motifs for distinguishing SOD classes and suggest general targets for anti-bacterial immune responses. The identified functional contributions, motifs, and targets distinguishing bacterial and eukaryotic SOD assemblies presented here provide a foundation for efforts to develop SOD-specific inhibitors or vaccines against these harmful pathogens.

IMPORTANCE. By protecting microbes against reactive oxygen insults, Cu,Zn superoxide dismutases (SODs) aid survival of many bacteria within their hosts. Despite the ubiquity and conservation of these key enzymes, notable species-specific differences relevant to pathogenesis remain undefined. To probe mechanisms that govern the functioning of *Neisseria meningitidis* and *Brucella abortus* SODs, we used X-ray structures, enzymology, modeling and murine infection experiments. We identified virulence determinants common to both homologs, assembly differences and a unique metal reservoir within meningococcal SOD that stabilizes the enzyme and may provide a safeguard against copper toxicity. The insights reported herein provide a rationale and basis for SOD-specific drugs and extension of immunogen design to target two important pathogens that continue to pose global health threats.

INTRODUCTION

Superoxide dismutases are master scavengers of reactive oxygen species (ROS), which are unavoidable byproducts of aerobic life. ROS, such as superoxide anion ($O_2^{\cdot-}$), H_2O_2 and $HO^{\cdot}$ play critical and varied roles in biological processes ranging from aging and oncogenesis, to pathogenesis and antibiotic action (1-4). ROS act as signals at low levels but as cytotoxins at higher levels (3, 5-8), so virtually all aerobic (and many anaerobic) organisms have evolved

Journal of Bacteriology JB Journal of Bacteriology

Accepted Manuscript Posted Online

Journal of Bacteriology

JB

Journal of Bacteriology

70 defenses for ROS detoxification. The superoxide dismutase enzymes, which catalyze dismutation
71 of $O_2^{\cdot-}$ radicals, are one such important antioxidant defense (9, 10). Three structurally distinct
72 families employ alternate oxidation and reduction of active-site metal ion cofactors (11) (Mn/Fe,
73 Ni, or Cu coupled to Zn) to protect different subcellular compartments (10). Ubiquitous
74 Cu,ZnSOD (herein after referred to as SOD) family members exhibit a Greek-key β-barrel fold
75 (12, 13) and can exist as monomers, dimers or tetramers of distinct assemblies, depending on the
76 particular enzyme (12, 14-17). All employ similar mechanisms to achieve their catalytic activity
77 and remarkable diffusion-limited reaction rates (18-22). However, our comparative mechanistic
78 analyses of the periplasmic SOD from *Photobacterium leiognathi* with the cytoplasmic
79 eukaryotic SODs suggested that some functional properties of bacterial (historically termed
80 prokaryotic or P-class) and eukaryotic (E-class) SODs (19) evolved independently. Notably,
81 periplasmic SODs are one of several defenses used by pathogenic bacteria to protect themselves
82 from the respiratory burst of their host's innate immune response, and thus to support bacterial
83 survival and replication within phagocytes (23-25).

84 *Neisseria meningitidis* and *Brucella abortus* are two major pathogens that continue to
85 threaten public health and welfare. The opportunistic bacterium *N. meningitidis* colonizes the
86 nasopharyngeal mucosa; its access to the blood can cause life-threatening infections. *N.*
87 *meningitidis* is a leading cause of meningitis and septicemia, with an estimated 1.2 million cases
88 of human meningococcal infection annually (26), but with non-uniform global distribution rates
89 (27), serogroup prevalences (28) and affected populations (29). Another gram-negative species,
90 *B. abortus*, is one of a handful of *Brucella* species producing the zoonotic disease brucellosis,
91 characterized by abortion, predominantly in ruminant animals including cattle, bison, sheep and
92 goats. Furthermore, although human brucellosis is well-controlled in the U.S. [~100 cases

Accepted Manuscript Posted Online

Journal of Bacteriology

JB

Journal of Bacteriology

93 reported annually], more than half a million new cases are diagnosed globally each year (30).
94 Infection is mostly due to laboratory contact, animal handling or consumption of tainted meat or
95 dairy products; human symptoms range from flu-like to arthritis, epididymal/testicular
96 inflammation, endocarditis, hepatitis and/or meningitis (31). Brucellosis therefore remains a
97 worldwide threat both to human health and to the livestock industry. Preventative strategies
98 against meningococcal disease and brucellosis have been met with some recent success.
99 Vaccines against the major *N. meningitidis* serogroups infecting humans are now available,
100 although their use is not routine, and their long-term efficacy has not been fully established in all
101 populations (32). Similarly, although several *B. abortus* vaccines are available for cattle and
102 small ruminants, their efficacy is variable and not protective against all *Brucella* species, with
103 some vaccines complicating serological testing and/or causing abortion in a percentage of
104 animals (33, 34). Further, no vaccine against human brucellosis currently exists (35). Thus,
105 research on understanding the host immune response to *N. meningitidis* and *B. abortus* is needed.
106 Cytoplasmic superoxide dismutases protect aerobic organisms from endogenous $O_2^{\cdot-}$-induced
107 damage to cellular enzymes (3, 4), and periplasmic SODs protect bacteria from extracytosolic
108 damage (36), which although less well characterized, can arise from $O_2^{\cdot-}$ produced endogenously
109 (37) or exogenously by phagosomal NADPH oxidases (38). Unsurprisingly, many pathogenic
110 SODs are potent virulence factors (39-43). Previously, we found that *N. meningitidis* SOD
111 (NmSOD) deletion mutants were much more sensitive than wild type (WT) to extracellularly
112 generated $O_2^{\cdot-}$ *in vitro* (44). Further, NmSOD mutant strains had increased phagocytic uptake
113 into monocytes/macrophages (45), and were also less virulent in mice (44). Similarly, *B. abortus*
114 SOD (BaSOD) deletion mutants were found to be susceptible to $O_2^{\cdot-}$ mediated killing *in vitro* and
115 by macrophages in mice (46) and exhibited decreased survival during initial phases of infection

Accepted Manuscript Posted Online

Journal of Bacteriology

JB

Journal of Bacteriology

(47). Furthermore our work found that immunization with a synthetic peptide derived from BaSOD was immunoprotective in mice (48). Supporting and extending these previous results we now show that neutralization of NmSOD with a monoclonal antibody (49), also protected mice during infection.

To better understand the molecular bases of virulence imparted by pathogenic SODs, we solved 7 high-resolution structures from *N. meningitidis* and *B. abortus.* By combining crystallography with small-angle X-ray scattering (SAXS) to obtain accurate structures, conformations and assemblies in solution (50), we found that NmSOD adopts a P-class dimeric assembly, whereas BaSOD functions as a monomer. An auxiliary Cu-binding site spanning the NmSOD dimer interface was found to contribute to enzyme stability and may promote survival of *N. meningitidis* within phagocytes. The Cu site geometries within the NmSOD and BaSOD structures indicate a mixture of oxidation states that promote SOD function within the phagosome. Our combined structural, mutational and biochemical analyses show that NmSOD K91 and K94 contribute to electrostatic substrate guidance to the catalytic Cu site. These data further highlighted motifs distinguishing P-class SODs from classic E-class SOD dimers. Collectively, these results expand our molecular-level understanding of bacterial SODs and suggest testable experimental and therapeutic strategies to target bacteria to prevent and treat pathogenesis.

MATERIALS AND METHODS

Protein expression and purification. NmSOD was overexpressed in *Escherichia coli* strain QC779 (51) by using the vector pJSK205 (44). *E. coli* in mid-log phase grown in LB medium were induced with 0.4 mM IPTG, and protein expression proceeded overnight. Overexpressed

Accepted Manuscript Posted Online

SOD directed to the periplasm was isolated by osmotic shock using 20% sucrose, precipitation using 65% (w/v) ammonium sulfate and subsequent centrifugation. The pellet was resuspended in 20 mL H_2O and dialyzed against H_2O for 4 hours at 4°C. The sample was then centrifuged for 30 min (8,000 x g), and $CuSO_4$ was added to the supernatant to a final concentration of 1 mM. The supernatant was then heated to 65°C for 30 min and then centrifuged for 45 min (40,000 x g). The supernatant was dialyzed against 20 mM MES, pH 5.9, and loaded onto a POROS 20 HS (Applied Biosystems) cation exchange column. Protein was eluted with a linear NaCl gradient, and SOD-containing fractions were pooled and dialyzed into 20 mM Tris-HCl, pH 8.0, and then applied to a POROS 20 HQ (Applied Biosystems) anion exchange column. Protein was eluted with a linear NaCl gradient, and fractions containing SOD were pooled, concentrated and applied to a HiLoad 16/600 Superdex 75 PG (GE Healthcare) gel filtration column. Peak fractions were pooled, and metal reconstitution with Cu and Zn was carried by dialysis as previously described (52). BaSOD was purified as described previously (53, 54). SOD activity of the recombinant proteins was measured using a gel-based SOD assay as described (11), and active, metal-reconstituted SOD aliquots were frozen in liquid nitrogen and stored at -80°C. NmSOD mutants (E73A, K91Q, K91E, K91Q/K94Q and K91E/K94E) were constructed in pJSK205 using the QuikChange site-directed mutagenesis kit (Agilent) and purified as described above for WT NmSOD. Human SOD (HsSOD) was prepared as described (55).

Protein analysis. Prior to SAXS analyses, analytical gel filtration was performed at 4°C on BaSOD, loaded at 9 mg/mL, and HsSOD, loaded at 10 mg/mL, onto a Superdex 75 10/300 GL column (GE Healthcare) in 20 mM Tris, pH 7.5, containing 500 mM NaCl with 2% glycerol. Molecular weight standards (Bio-Rad) were run in the same buffer for comparison. A similar elution profile for monomeric BaSOD was also obtained on a 120 x 2.5 cm Sepharose G-75

Journal of Bacteriology JB Journal of Bacteriology

Accepted Manuscript Posted Online

column using 10 mM sodium-potassium phosphate, pH 6.4, 150 mM NaCl.

For metal analysis, samples of NmSOD were digested with concentrated nitric acid for 2 hours at 65° C, and were then diluted to 10% nitric acid with distilled H_2O for Inductively-Coupled Plasma Optical Emission Spectrometry (ICP-OES) analysis on a Vista-MPX Spectrophotometer (Varian). Metal content was determined from 3 independent wavelengths, by using standard curves for Cu and Zn (0.1 to 100 ppm). The protein concentrations of the samples prior to digestion were determined by UV absorbance, and were used together with the ICP-OES results to determine the metal:protein ratio for NmSOD samples.

Stability measurements were performed as described previously (56) by titration of purified WT and E73A NmSOD samples and WT HsSOD (final concentration of 20 μM) with guanidine-HCl (from 0 to 7 M, in 0.5-M steps) in the presence of PBS, pH 7.4, subsequent vortexing and overnight incubation at room temperature, followed by circular dichroism (CD). The CD sample cell path length was 0.1 cm, and the ellipticities were measured at 218 nm in an AVIV model 2o2SF stopped-flow CD spectrometer in kinetics mode. Three 30-second measurements were averaged to obtain the final values, and Equation 1 was used to convert the raw CD data into fraction unfolded (Fu) for normalization:

$$Fu = \frac{(Y_n - Y)}{(Y_n - Y_d)} \quad (1)$$

Y_n and Y_d are the intercepts of the lines through the lower and upper plateau regions (low and high denaturant concentrations), respectively, and Y is the CD value at a given concentration of guanidine-HCl. Data were plotted as fraction unfolded versus guanidine concentration by using Origin 5.0 (Microcal Software Inc.) and fit to a sigmoidal curve. Detailed analyses of the free-energy changes were not included, as previous work suggests that WT SOD folding and unfolding are not entirely reversible because of metal binding (56).

Journal of Bacteriology JB Journal of Bacteriology

Accepted Manuscript Posted Online

For pulse radiolysis measurements, all solutions were prepared using ultra-purified (Millipore) distilled water, and reaction rates of SOD with $O_2^{\cdot-}$ were measured using the 2-MeV Van de Graaff accelerator at Brookhaven National Laboratory. Dosimetry was calculated using the KSCN dosimeter with a molar extinction coefficient of 7950 $M^{-1}cm^{-1}$ for $(SCN)_2^-$ and a G value of 6.13. The path length was 2 cm, and a radiation dose of 150-2000 rads was used, yielding 1-20 μM $O_2^{\cdot-}$ per pulse. All activity measurements were carried out using aqueous solutions containing 10 mM formate, 10 mM phosphate at 25° C. The first measurement was made in the absence of ethylenediaminetetraacetic acid (EDTA), and subsequent measurements were made after adding 10 μM EDTA. No difference was observed in disproportionation rate, ensuring that no free Cu was present to confound the results.

The radiolysis of water predominantly yields e_{aq}^-, OH and H. These radicals can be converted to $O_2^{\cdot-}$ radical by the following reactions: $e_{aq}^- + O_2 \rightarrow O_2^{\cdot-}$; $OH/H + HCO_2^- \rightarrow H_2O/H_2 + CO_2^-$; and $CO_2^- + O_2 \rightarrow O_2^{\cdot-} + CO_2$. The disappearance of $O_2^{\cdot-}$ was followed spectroscopically at 260 nm [$\varepsilon(O_2^{\cdot-})$ = 1800 $M^{-1}cm^{-1}$ at 260 nm] in the absence and presence of micromolar concentrations of enzyme. EDTA and sodium formate were purchased from Sigma and monobasic potassium phosphate from Ultrex, JT Baker, Inc. Solution pH was adjusted by adding H_2SO_4 (double distilled from Vycor, GFC Chem. Co.) and NaOH (Puratronic, Alfa/Ventron Chem.).

The activities of BaSOD and bovine erythrocyte SOD (Sigma) were assessed by using the xanthine/xanthine oxidase system as previously described (57).

X-ray crystallography. Crystals of NmSOD (WT and mutants) and BaSOD were obtained from 2-2.3 M $(NH_4)_2SO_4$, pH 6-8.0, and 100-200 mM KCl by using the hanging drop vapor diffusion method, with the exception of the NmSOD E73A mutant, which was crystallized from 20% polyethylene glycol 3000, 50 mM Tris-HCl, pH 8.0. Prior to cryogenic cooling, crystals

Journal of Bacteriology JB Journal of Bacteriology

Accepted Manuscript Posted Online

were soaked in a solution of 20% (v/v) glycerol, 75% (w/v) saturated $(NH_4)_2SO_4$, 50 mM Tris, pH 7.5, 50 mM NaCl, 0.1 mM EDTA, and 0.02% NaN_3, except for NmSOD E73A, which was soaked in mother liquor plus 20% ethylene glycol.

Diffraction data for all crystals were collected at the Stanford Synchrotron Radiation Laboratory (SSRL). Table S1 lists the specific beamlines used for each dataset. Data reduction and processing were carried out using the HKL package (HKL Research, Charlottesville, VA). Initial phases for NmSOD and BaSOD were obtained by molecular replacement using AMoRE (58) with *A. pleuropneumoniae* SOD [ApSOD; RCSB Protein Data Bank (PDB) code: 2APS] and a monomer of *S. typhimurium* SodCI (PDB code: 1EQW), respectively. The best scoring repositioned models were refined in CNS (59). Each subunit was treated as a rigid body for the initial refinements, and then the structures were refined using torsion angle simulated annealing at 5,000 K. Following these initial stages, the refinement of the models proceeded through cycles of manual rebuilding in XFIT (60) into sigma-A–weighted $2F_o$-F_c and F_o-F_c electron density maps, and then positional and temperature factor refinement. Composite-omit simulated annealing maps were calculated for fitting when needed. The maximum likelihood target function, bulk solvent corrections and anisotropic temperature factor corrections were used for the refinement cycles in CNS. Where resolution permitted, the structures were then further refined using SHELXL (61) and the same R_{free} reflection set along with individual anisotropic temperature factors. PHENIX (62) was used in the final round of refinement for BaSOD.

Small-angle X-ray scattering (SAXS). Solution scattering data on WT NmSOD and BaSOD were collected at SIBYLS beamline 12.3.1 at the Advanced Light Source of Lawrence Berkeley National Laboratory (63). Both samples were subjected to size-exclusion chromatography using a Superdex 75 10/300 GL column (GE Healthcare) prior to SAXS

Journal of Bacteriology JB Journal of Bacteriology

Accepted Manuscript Posted Online

analysis. SAXS data were collected on 15-µL samples at 16°C, using automated sample loading from a 96-well format and a MAR CCD 165 detector with a sample-to-detector distance of 1.5 m. The X-ray wavelength (λ) was 1.03 Å, and the scattering vector q ($q = 4\pi \sin\theta/\lambda$, where 2θ is the scattering angle) range was ~0.01 to 0.32 $Å^{-1}$. X-ray exposures ranged from 0.5 to 5 seconds (for each sample and matching gel filtration buffer blank), and the scattering of the buffer was subtracted from that of the protein. NmSOD was analyzed at 1.18, 1.3 and 2.35 mg/mL in phosphate-buffered saline (pH 7.4) containing 2% glycerol, and profiles superimposed well. X-ray exposure data for the 1.3 mg/mL sample were used for merging and further analyses. BaSOD was run at 0.85 and 1.7 mg/mL in 20 mM Tris, pH 7.5, containing 500 mM NaCl with 2% glycerol, and data at 1.7 mg/mL were used for further analyses. Data sets were merged with PRIMUS (64). The $P(r)$ function, R_g (real space approximation) and maximum distance D_{max} were calculated with GNOM (65). DAMMIF (66) was used to generate 10 *ab initio* models each for NmSOD and BaSOD, which were then averaged using DAMAVER (67). Further details are tabulated in Table S2. FoXS (68) was used for theoretical profile computation and data fitting.

Molecular image rendering and modeling. PyMOL (Schrodinger, LLC) and Chimera (69) were used for generating structural images. The ClustalOmega server (http://www.ebi.ac.uk/Tools/msa/clustalo/) was used for sequence alignment. Normal mode analysis (NMA) models were generated using default settings on the elNémo server (70).

Structural coordinates. The coordinates described in this paper were deposited into the PDB: NmSOD (2AQN), NmSOD E73A (2AQP), NmSOD K91Q (2AQR), NmSOD K91E (2AQQ), NmSOD K91Q/K94Q (2AQT), NmSOD K91E/K94E (2AQS) and BaSOD (4L05). SAXS data were deposited into the BIOISIS repository (bioisis.net) using codes NMSODP and BASODP.

Journal of Bacteriology JB Journal of Bacteriology

Accepted Manuscript Posted Online

Antibody, bacterial strains and animal studies. The mouse monoclonal antibody HD1 was previously described (49). *N. meningitidis* MC58 (B:15:P1.7,16-2, ST-74, cc32) wild type and *sodC* knockout strains were cultured as described (44), and Western blotting was used to detect binding of HD1 to *N. meningitidis* protein extracts separated by denaturing or non-denaturing gel electrophoresis. Mice were challenged with 2 x 10^6 cfu intraperitoneal *N. meningitidis* co-administered with or without HD1 antibody, as described previously (44). Survival was monitored for 4 days post infection. All animal-related studies were conducted under guidelines approved by the IACUC of the USDA National Animal Disease Center or by the Home Office, UK.

NmSOD deletion mutants and HD1 epitope analysis. NmSOD deletion constructs were constructed by PCR. The encoded protein sequence of the C-terminal deletion mutant (lacking 9 residues) was MKYLLPTAAAGLLLLAAQPAMAHGHGHGHGHGHEHNTIPKGASIEVKVQQLDPVNGN KDVGTVTITESNYGLVFTPDLQGLSEGLHGFHIHENPSCEPKEKEGKLTAGLGAGGHWD PKGAKQHGYPWQDDAHLGDLPALTVLHDGTATNPVLAPRLKHLDDVRGHSIMIHTGG DNHSDHPAPLGGGG, and that of the internal deletion mutant (lacking 71 residues) was MKYLLPTAAAGLLLLAAQPAMAHGHGHGHGHGHEHNTIPKGASIEVKVQQLDPVNGN KDVGTVTITESNYGLVFTPDLQGLSEGLHGFHIHENPSCEPKEKEGKLTAGLGAGGHWD PRMACGVIK.

Deletion mutants were expressed in *E. coli* as described above. To confirm gene expression, RNA was prepared, and RT-PCR was performed using oligonucleotide primers for the respective *sodC* genes. As previously reported, immobilized metal affinity chromatography can be used to purify histidine-rich SOD samples (71). Whole cell lysates were applied to cobalt-Talon resin

Journal of Bacteriology JB Journal of Bacteriology

Accepted Manuscript Posted Online

Journal of Bacteriology

JB

Journal of Bacteriology

277 (Clontech), and activity of the eluted NmSOD samples was assessed as described previously
278 (44). Western blotting was used to detect binding of HD1 to deletion mutants.
279
280 **RESULTS**
281 **Anti-SOD antibody provides protection from *N. meningitidis* infection.** To test the
282 hypothesis that NmSOD is a virulence factor that protects meningococci from free-radical
283 mediated host defenses, we examined the ability of a monoclonal anti-SOD antibody to passively
284 protect mice against *N. meningitidis* challenge. Passive immunity provides immediate, rather
285 than delayed, protection against infection, and is currently used for post-exposure prophylaxis for
286 chicken pox (*Varicella Zoster*) and rabies in humans (72, 73). In our experiments, mice were
287 challenged with a dose of 2 x 10^6 cfu of *N. meningitidis* (MC58), with or without co-
288 administration of the monoclonal NmSOD-reactive antibody HD1 (49), and subsequently
289 monitored for survival. Our results demonstrated that this NmSOD-neutralizing antibody
290 conferred a robust level of passive protection, with a survival rate of 100% in HD1-treated mice
291 at 4-days post-infection (Fig. 1).
292 ***N. meningitidis* Cu,Zn superoxide dismutase (NmSOD) conserves P-class dimer**
293 **assembly.** To better understand potential determinants of virulence for NmSOD, we solved the
294 structure of the enzyme to 1.4-Å resolution (Table S1; R_{work} = 12.8%, R_{free} = 19%). Each subunit
295 of the NmSOD homodimer conserves the SOD Greek-key β-barrel fold (Figs. 2 and 3): the root-
296 mean-square-deviations (RMSDs) of Cα atoms between NmSOD and bacterial SOD structures
297 from *Actinobacillus pleuropneumoniae* (PDB code: 2APS) (74), *Haemophilus ducreyi* (1Z9N)
298 (75), *P. leiognathi* (1YAI) (19, 76, 77), *Salmonella typhimurium* SodCI (1EQW) (78) and
299 *Yersinia pseudotuberculosis* (2WWO) were all < 1 Å. As suggested by comparative structural

Accepted Manuscript Posted Online

Journal of Bacteriology

JB

Journal of Bacteriology

analyses of bacterial SOD sequences (Fig. S1) (74), subunit interface residues characteristic of dimeric P-class SODs were conserved in NmSOD (Fig. 3C), together with the ring-like assembly of buried water molecules (Figs. 2A and 3B). The surface buried by the dimer interface was calculated with PISA to be to be ~915 Å^2. This P-class dimer is the best-represented crystallographic assembly for bacterial SODs in the Protein Data Bank thus far (Table S3).

To determine whether the biological state of the enzyme is accurately represented within the crystal, we used SAXS, which allows determination of conformations and assemblies for macromolecules in solution (79, 80). NmSOD SAXS data agreed with scattering profiles predicted from the crystallographic dimer, with a χ^2_{free} value (80) of 1.83 (Fig. 2D). The SAXS-derived electron pair distribution [P(r) plot] (Fig. 2E) and molecular envelope models (Fig. 2F, left) further indicated an elongated shape consistent with the crystal structure. SAXS measurements also indicated a marginally lower-than-average particle density (81) for NmSOD (Table S2), with small deviations in the profile fit for scattering angles > q = 0.17 (Fig. 2D). These observations, also supported by normal mode analyses (Fig. S2) and elevated (atomic displacement parameters, ADP; B-factors), suggested considerable protein flexibility in NmSOD, particularly within bacterial SOD-specific loop regions (Fig. S3).

Electrostatic guidance in NmSOD speeds enzymatic activity. The crystal structure of NmSOD revealed that seven, conserved, active-site residues mediate Cu (histidines H79, H81, H104 and H160) and Zn (H104, H113, H122 and aspartic acid D125) coordination (Figs. 2C and S1). The catalytic Cu site has trigonal planar ligation geometry characteristic of reduced Cu(I), as was also found in structures of E-class yeast SOD (PDB code: 2JCW) (82) and P-class *A. pleuropneumoniae* SOD (PDB code: 2APS) (74), among others. The average Cu(I)–ligand bond lengths (± standard deviation) for the 3 NmSOD subunits in the asymmetric unit were 2.0 ± 0.0,

Accepted Manuscript Posted Online

Journal of Bacteriology

JB

2.0 ± 0.1 and 2.0 ± 0.1 Å for H79, H81 and H160, respectively. The 3.1 ± 0.1-Å separation distance between Cu(I) and H104 indicates a broken bond to the bridging histidine, which ligates both metal ions in the oxidized enzyme. The Zn site exhibits a characteristic, distorted tetrahedral geometry, with average bridging H104-Zn distance of 2.0 ± 0.1 Å.

Analyses of SOD structures and sequences suggested that residues promoting electrostatic guidance in bacterial SODs lie across the active-site channel from the functionally equivalent electrostatic loop (linking β-strands 7 and 8) of eukaryotic SODs (19, 74). The functionally equivalent NmSOD residues predicted from our structural alignment (Fig. S1) include K91, E92 and K94, located in a bacterial SOD sequence insertion (relative to eukaryotic SODs, Fig. 3C), forming a protruding β-hairpin at the ends of P-class dimer (Fig. 2A). We constructed mutants to either neutralize (K91Q and K91Q/K94Q) or reverse (K91E and K91E/K94E) one or both charges, and then used pulse radiolysis to evaluate the rate constants over a wide pH range (Fig. 4A). We found that while charge neutralization at residue 91 alone did not substantially affect the rate constant, the K91Q/K94Q double mutant reacted 1.5-fold more slowly than WT. Moreover, reversing the charge at one or both residues decreased the rate constant substantially: At pH 7, the rate constants for K91E and K91E/K94E dropped 2.5-fold and 5-fold, respectively, relative to that for WT (Fig. 4A). Mirroring analogous studies on the HsSOD enzyme (18), these results confirmed the involvement of these two lysine residues in the electrostatic attraction of $O_2^{\cdot-}$ substrate to the active-site Cu ion in NmSOD and suggest a greater contribution for K94 than was seen for the equivalent residue in the monomeric *E. coli* enzyme (83). We also determined structures of these NmSOD electrostatic mutants at resolutions ranging from 1.65 to 1.8 Å (Fig. S3 and Table S1). Apart from mutation site alterations (most notable in K91E/K94E), slight subunit rotations and modestly increased ADPs (Fig. S3B), all structures were similar to WT

Journal of Bacteriology

Accepted Manuscript Posted Online

Journal of Bacteriology

JB

Journal of Bacteriology

346 (Fig. S3A). These findings suggest that fine-tuning of electrostatic guidance is not accomplished
347 through major structural rearrangements in NmSOD, and also confirm that the active site
348 geometry is maintained in the mutants described above.
349
350 **A stabilizing, auxiliary copper site bridges the NmSOD dimer interface.** Metal sites are
351 key contributors of activity and stability in SODs. Surprisingly, ICP-OES analyses of NmSOD
352 indicated a stoichiometry of 1.5 Cu ions per subunit, matching one in each active site and one
353 additional Cu ion per dimer. Correspondingly, in the X-ray structures (Figs. 2 and 4), we
354 observed a unique, cross-dimer, Cu-binding site, evidenced by a strong (> 10σ) electron density
355 peak in omit maps (Figs. 2A, S4B, 4C, top, and 4D). This auxiliary Cu is tetrahedrally ligated by
356 H133 and E73 from each subunit (Figs. 4C, top, and 5A), implying an oxidized Cu(II) state.
357 Thus, the NmSOD structure appears to contain both oxidized and reduced Cu sites, suggesting
358 that the geometry of these sites tunes their redox activity; the distorted active-site Cu ion
359 geometry evolved to promote redox chemistry for catalysis, whereas the less-constrained
360 geometry of the auxiliary site allows the Cu ion to remain oxidized, despite equivalent exposure
361 to reduction by free electrons during the X-ray diffraction data collection. Interestingly,
362 structural superposition of NmSOD with *H. ducreyi* SOD (HdSOD), which contains an unique
363 heme-binding site (75, 84) revealed that the auxiliary Cu and heme Fe align, each forming an
364 unusual cross-dimer bridge (Fig. 4D-E).
365 To probe the functional contributions of the auxiliary Cu in NmSOD, we constructed the
366 E73A point mutant, which removed 2 ligands from the cross-dimer Cu-binding site. We found
367 no major oligomeric state (Fig. S4A) or catalytic differences between WT and E73A NmSOD,
368 aside from a slight rate increase for E73A NmSOD above pH 8.5 (Fig. 4A). Next, to assess

Accepted Manuscript Posted Online

Journal of Bacteriology

JB

Journal of Bacteriology

whether the auxiliary Cu-binding site affects protein stability, we used circular dichroism (CD) spectroscopy to monitor NmSOD unfolding, under increasing concentrations of guanidine-HCl (Gu-HCl) (Fig. 4B). Generally, the unfolding curves for WT and E73A NmSOD were less steep than that for WT HsSOD, suggesting somewhat less concerted and cooperative unfolding for the bacterial enzyme. WT NmSOD and HsSOD displayed similar unfolding, with the NmSOD unfolding midpoint marginally greater (4.3 M Gu-HCl) than that of HsSOD (3.9 M). E73A unfolded at a slightly lower concentration of guanidine-HCl (3.6 M), indicating a modest loss of stability upon removal of Cu-binding E73. Unfolding of E73A also began at lower Gu-HCl concentrations than for either WT enzyme, and complete unfolding of WT NmSOD required higher Gu-HCl concentrations, relative to WT HsSOD or E73A NmSOD. Overall, these results suggest that although the auxiliary, dimer-spanning, Cu-binding site it is not necessary for dimer formation, it stabilizes the NmSOD assembly.

To understand how E73 imparts stability at the atomic level, we determined the crystallographic structure of E73A NmSOD to 1.3-Å resolution (Fig. 4C, bottom and Table S1; R_{work} = 13.5, R_{free} = 18.3). We found that the E73A NmSOD structure was generally similar to WT, but with no Cu bound in the vicinity of A73 (Fig. 4C, bottom). Instead, Cu ions appeared to mediate crystal contacts between H148 of one E73A NmSOD dimer and its symmetry mate (Fig. S4C). In contrast, mutation of electrostatic guidance residues did not affect the position of the auxiliary Cu ion in NmSOD (Fig. S3B), despite differing crystal symmetries and solvent contents (Table S1). These results suggest that the decreased stability arises from the lack of Cu binding, rather than from gross structural differences.

***B. abortus* Cu,Zn superoxide dismutase (BaSOD) has a conserved active site but monomeric assembly.** Sequence alignments suggested that BaSOD, in contrast to NmSOD,

Accepted Manuscript Posted Online

Journal of Bacteriology

JB

lacks canonical P-class dimer interface residues (Fig. S1) (74), and NMR results suggested BaSOD was a monomer (53). Informed by these observations, we proceeded to solve the high-resolution X-ray crystallographic structure of BaSOD to 1.1-Å resolution (Table S1; R_{work} = 11.3, R_{free} = 13.8). Notably, the active-site electron density of BaSOD revealed a mixture of oxidized and reduced structural conformations, reflective of the enzyme mechanism, so we modeled 2 positions each for the Cu ion and its bridging histidine (Fig. 2C, bottom). In the oxidized state, the bridging H73-Cu(II) bond is 2.0-Å long, and upon reduction, active-site movements shift the H73 side chain 3.1 Å away from Cu(I) such that H73 can form a 2.5-Å hydrogen bond with a bound water molecule within the active site. The bond distances between the 2 alternate H73 conformations and the Zn ion are 1.9 and 2.1 Å. For the remaining ligands, the Cu(I)–ligand bond lengths are 2.0, 2.0 and 2.1 Å for H48, H50 and H128, respectively, and Cu(II)–ligand bond lengths are 2.1, 2.2 and 2.2 Å for H48, H50 and H128, respectively. Like NmSOD, BaSOD retains the overall Greek-key β-barrel fold conserved in other Cu,ZnSODs (Fig. 2B) (85), albeit with only one BaSOD molecule contained within the asymmetric unit.

***B. abortus* SOD is active as a monomeric enzyme.** BaSOD exhibited activity similar to that of the well-studied bovine SOD dimer (Fig. S5A), even though the crystal structure suggested that BaSOD is monomeric. To confirm this stoichiometry, we used both gel filtration chromatography (Fig. S5B) and SAXS (Fig. 2D-E), which ascertained the monomeric biological assembly of the enzyme in solution. The SAXS profile (Fig. 2D) revealed that the BaSOD monomer in the crystallographic asymmetric unit matches the shape and assembly in solution (χ^2_{free} value of 1.30), and is distinct from the dimeric NmSOD SAXS profile; the P(r) plot and *ab initio* envelopes for BaSOD in solution (Fig. 2E-F) indicated a smaller, more globular shape that

Accepted Manuscript Posted Online

fit the monomeric crystallographic structure. Although diverse Cu,ZnSOD enzymes retain the same subunit fold and Cu-mediated chemistry, their quaternary assembly varies considerably, notably in bacteria (Table S3 and Fig. 3). Although SOD monomers are less well represented than P-class dimers in the PDB, the BaSOD structure is similar to monomeric homologs *E. coli* SOD (PDB code: 1ESO (86), with an R.M.S.D. of < 0.6 Å), *S. enterica* SodCII (2K4W (87), R.M.S.D. ~1.4 Å) and *Bacillus subtilis* SOD-like protein (1S4I (88), R.M.S.D. ~1.08), with discrepancies predominantly in loop regions. Overall, monomeric SODs are stable and active, despite the prevalence of their dimeric counterparts.

Epitope mapping onto NmSOD and BaSOD structures. The crystal structures and resulting structure-based sequence alignments of NmSOD and BaSOD enabled us to investigate the determinants of virulence within these enzymes. The anti-SOD antibody HD1 (49) bound strongly to NmSOD in denaturing or non-denaturing Western blots of *N. meningitidis* protein extracts, and we established that no cross-reactive meningococcal products bound HD1 by using a *sodC* knockout strain. Given the cross-reactivity of HD1 to several known bacterial SODs and (49) and the high sequence conservation in the C-terminus, we hypothesized that this region might contain the HD1 epitope. To test this prediction, we created 2 NmSOD deletion mutants (see Materials and Methods): a 9-residue C-terminal deletion mutant (which disrupts the disulfide loop) and an internal deletion mutant that retained this C-terminal sequence (Fig. S6). The mutant proteins were expressed in *E. coli*, and then tested for SOD activity and HD1 reactivity. Both proteins lacked dismutase activity, but only the internal deletion mutant bound HD1 in Western blots. These binding results suggest that the C-terminal residues contribute to the NmSOD epitope recognized by the HD1 antibody, which protected mice from succumbing to *N. meningitidis* infection (Figs. 1 and S6). The 9-residue C-terminal NmSOD sequence

Journal of Bacteriology JB Journal of Bacteriology

Accepted Manuscript Posted Online

Journal of Bacteriology

JB

(PRMACGVIK) includes 6 residues conserved across domains of life, as well as variable residues (xRxACGVIx) that may dictate the reactivity of HD1. In NmSOD, the first and third variable residues of this sequence flank the invariant active-site arginine to form a "PRM" motif shared by HD1-reactive (49), dimeric SODs from *Actinobacillus* and *Haemophilus*. In contrast, the monomeric BaSOD and *E. coli* SODs do not react with HD1 (49) and lack the "PRM" motif within the proposed C-terminal epitope of HD1 (Fig. S6).

To understand the structural basis for protective peptide immunogens in BaSOD, we mapped the peptide immunogens we had previously tested (48) onto our structure (Fig. S7). The protective BaSOD peptide (residues 56-67, Fig. 3C, underlined in red) occurs in the loop insert specific to the bacterial SODs (Fig. 3C, boxed) that contains electrostatic guidance residues K60, D61 and K63. Comparison of this loop in the bacterial and HsSOD structures (and by analogy murine SOD) revealed an extended protrusion in BaSOD (and NmSOD) (Fig. 6). Therefore, antibody binding to this BaSOD epitope would be expected to disrupt electrostatic guidance and/or sterically hinder access to the active site. In contrast, the 2 non-protective peptides span residues 117-131 and 130-143 (Fig. S7, orange). The former encompasses all of strand β_7 [numbered going around the β-barrel (74)] and part of the core β-barrel framework forming the back wall of the active site (containing Cu ligand H128). This epitope is only partly solvent-exposed; therefore, an immune response to the intact protein might not be expected. The latter non-protective peptide encompasses part of the loop connecting strand β_7 to strand β_8 (the electrostatic loop of eukaryotic SODs). This surface-exposed loop is adjacent to the active site, but is not critical to enzymatic functioning of bacterial SODs, so antibody binding may only modestly impact substrate entry. These BaSOD peptide vaccines were developed based on hydrophobicity, flexibility and antigenicity predictions, in the absence of any structural

Journal of Bacteriology

Accepted Manuscript Posted Online

Journal of Bacteriology

JB

Journal of Bacteriology

information (48). The high-resolution structures presented here provide detailed, specific frameworks to improve targeting for the development of more effective vaccines.

DISCUSSION

Structural insights differentiating bacterial and eukaryotic Cu,ZnSODs. The oligomeric state of a protein can control its physicochemical properties, behavior and biological interactions, and thus is key for informed design of drugs and vaccines. For example, HsSOD polymers genetically engineered for therapeutic use as anti-inflammatories exhibited a desirable extended serum half-life (89); conversely, loss of assembly specificity in mutant HsSODs was associated with toxic aggregation in the degenerative motor neuron disease Amyotrophic Lateral Sclerosis (ALS) (55, 56). Many distinct assemblies have been found for the Cu,ZnSOD subunit fold (Fig. 3A): the bacterial P-class monomer and dimer, an alternative extended-loop dimer found in *Mycobacterium tuberculosis* SodC (90) (herein termed Loop or L-class) and the *B. subtilis* SOD-like dimer (88) (Table S3); and in eukaryotes, a fungal monomer (91), the metazoan E-class dimer (12) and the dimer-of-dimers tetramer of extracellular SOD (17), as well as larger "dogbone" (12) and nanofilaments (92) assemblies of HsSOD dimers. Determining the natural biological assembly state from a crystallographic structure can be challenging, especially for SOD proteins, which display these different biological assemblies and many complex crystal packing arrangements. Therefore, complementary characterization in solution is crucial for accurately defining the physiological assembly state of a protein (93, 94), as we report here for the architecturally distinct virulence factors NmSOD and BaSOD (Fig. 2).

Exploitable physiological differences between bacterial and eukaryotic SODs stem from evolutionary structural dissimilarities. Here, based on our new structures, we identify sequence

Accepted Manuscript Posted Online

Journal of Bacteriology

JB

Journal of Bacteriology

484 motifs that discriminate among SOD homologs, assign stoichiometry and connect gene to
485 function (Figs. 3C and S1). Two conserved motifs identify most CuZnSODs: a C-terminal
486 RX(A/V/S)CGV(I/V) sequence (Figs. 3C and S1), and the active-site histidine pattern, notably
487 the first 2 Cu-ligating histidines separated by a single hydrophobic residue. So, how are bacterial
488 SODs distinguished from those of eukaryotes? First, only E-class enzymes conserve an aromatic
489 (or hydrophobic) interface residue (F50 in HsSOD) followed by glycine, positioned 2 residues
490 after the second Cu-ligating histidine, as well as a salt-bridging arginine (R79 in HsSOD),
491 positioned immediately before the third Zn-binding histidine. Another feature is the C-terminal
492 shift of the first disulfide bond cysteine, arising from a disulfide loop insertion in bacterial SODs.
493 In P-class SODs, this cysteine is positioned 5 residues after the second Cu-ligating histidine,
494 while in E-class SODs, it is 6 residues before the third Cu-ligating (bridging) histidine (Fig. 3C).
495 In bovine and HsSODs, mutation of oxidation-prone free cysteines (near the N-terminus and
496 Greek key connections) increased enzyme stability (12, 95). Notably, the P-class SODs lack free
497 cysteines, which are selected against in the oxidizing periplasm (96, 97); this feature may
498 contribute to the higher stability of NmSOD, relative to HsSOD (Fig. 4B). These insights extend
499 our previous work detailing the molecular basis of the Greek key β-barrel evolution (98).

500 Given the diversity among microbial SODs, we also re-evaluated sequence and structural
501 features characteristic of their different assembly states. L-class bacterial SODs are clearly
502 differentiated from their P-class counterparts by a large insertion between the last 2 β-strands,
503 but how are P-class dimers and monomers distinguished? P-class dimer interfaces generally
504 conserve 4 buried aromatic or hydrophobic residues encircling a buried water ring (19, 74-76)
505 (Fig. 3B and 3C, red): i) a lateral aromatic tryptophan or tyrosine (19, 74, 76, 78); ii) its cognate
506 hydrophobic residue (19, 74, 76, 78), typically V or L, in the opposing monomer; iii) a YG motif

Accepted Manuscript Posted Online

Journal of Bacteriology

JB

Journal of Bacteriology

present in a majority of P-class dimers, which forms hydrophobic packing interactions and a hydrogen bond with an adjacent D at the bottom of the interface (which variably interacts with residues adjacent to the YG) (19, 74, 76, 78), and iv) a hydrophobic amino acid, which contributes to a hydrophobic cluster toward the top of the interface through interactions with 1 (19, 76, 78) or more of its cognate residues in the opposing monomer. This cluster is located just below the auxiliary copper site in NmSOD (Fig. 3B). In P-class monomers, however, these 4 conserved residues are frequently replaced with hydrophilic or hydrogen-bonding residues expected to destabilize hydrophobic interface packing (86), which was echoed experimentally by characterization of monomer-dimer hybrid proteins (99). These discriminating features identified from SODs of known structure suggest that the assembly class is predictable from sequence data (e.g. for uncharacterized archaeal SOD-like sequences or SODs from bacterial and eukaryotic viruses that conserve P-class (41) and E-class (100, 101) features, respectively). Identification, testing and refinement of these predictive motifs show promise for distinguishing the SODs of pathogens from those of their hosts, for therapeutic targeting applications.

Significance of the auxiliary Cu site in NmSOD. The need to control ROS has been a major driver of pathogenic and eukaryotic evolution, with the extreme example of glutathione peroxidase incorporation of selenocysteine, via an altered stop codon (102). Cu-containing SODs evolved to protect against rising oxygen (103), thus allowing bacterial SODs to also serve as virulence factors protecting pathogens from ROS-mediated host defenses. Host phagocytes use an arsenal of strategies to combat bacterial invaders during engulfment and phagosomal maturation stages of infection (Fig. 5B). During the latter process, toxic levels of phagosomal Cu may contribute to bactericidal activity (104), in part through ROS production and resulting oxidative damage (105). N-terminal histidine- and/or methionine-rich Cu(I/II) and/or Zn(II)

Accepted Manuscript Posted Online

Journal of Bacteriology

JB

Journal of Bacteriology

binding motifs in *H. ducreyi* and *A. pleuropneumoniae* SODs (71, 106, 107) may facilitate Cu acquisition or active-site transfer in scarce conditions (106), and also serve to protect these pathogens from phagosomal Cu toxicity. Likewise, auxiliary metal (nickel and bismuth) binding sites in other bacterial proteins are implicated in metal buffering, sequestration and toxicity (108). The novel metal site at the NmSOD interface was unexpected, but is consistent with observations that microbial metalloproteomes are still incompletely characterized (109). These findings further our understanding of metal-buffering properties in key bacterial proteins.

Interestingly, the auxiliary NmSOD Cu site corresponds to the heme-binding site in HdSOD (75, 84) (Fig. 4D-E), with HdSOD ligands H64 and H124 positionally equivalent to NmSOD E73 and H133, although the HdSOD heme is bound asymmetrically. Since *H. ducreyi* cannot synthesize heme and must obtain it from its host, HdSOD was proposed to be involved in heme metabolism as a sensor or buffer against heme toxicity (75). Based on these similarities, we tested heme-binding to NmSOD *in vitro* by using the same procedure (84) but found no evidence of bound heme. The auxiliary Cu- and heme-binding residues are not generally conserved in other SODs (Fig. S1, red squares), highlighting the uniqueness of this interface region as a potential antimicrobial target. The solvent-exposed cavity (Figs. 3B and 5A) formed between the auxiliary Cu site and the rest of the P-class dimer interface makes an attractive target for small molecule binding. For instance, an inhibitor targeted to this cavity could disrupt binding of the auxiliary Cu, thus compromising NmSOD stability. CO or NO binding to the heme in HdSOD did in fact induce conformational rearrangements of that enzyme, including altered active-site accessibility (110). Similarly, active-site accessibility and catalysis were affected by interface substitution mutants in the *P. leiognathi* SOD P-class dimer (111). The slightly extended pH range over which NmSOD E73A was active (Fig. 4A) suggests that NmSOD interface

Accepted Manuscript Posted Online

Journal of Bacteriology

JB

Journal of Bacteriology

553 modulation might also alter catalytic activity through allosteric effects. Thus, our NmSOD
554 structures (Figs. 4C, 5A and S3-S4) provide an experimental basis for testing the impacts of the
555 auxiliary Cu site, not only on enzyme activity and stability, but also on virulence and survival of
556 this deadly pathogen.

557 **Protective immunity via targeting of bacterial SODs.** The monoclonal anti-SOD antibody
558 HD1 recognizes not only meningococcal SODs, but also ApSOD and *Haemophilus* SOD (49).
559 Here, we showed that HD1 conferred an impressive level of passive protection against infection
560 of mice with different strains of serogroup B meningococci (Fig. 1), and that the NmSOD C-
561 terminus is critical for HD1 binding (Fig. S6). Although the epitope recognized by HD1 has not
562 yet been comprehensively characterized, this antibody serves as both a useful experimental tool
563 and a proof of concept for protective immunization. In contrast, we were unable to confer active
564 protection in mice using a standard preparation of recombinant NmSOD. Thus, re-engineered
565 NmSOD or peptide fragments may provide useful components for broadening coverage of
566 existing vaccine formulations (112). Since the most common serogroups of *N. meningitidis* all
567 express the *sodC* gene (44) and NmSODs are highly sequence-conserved, a SOD immunogen
568 might also improve vaccine efficacy against related microbes.

569 Current animal vaccines for brucellosis are unsuitable for human use, and accidental
570 exposure to these brucellosis strains can result in adverse effects (113). The illegitimate use of
571 *Brucella* as a potential bioterrorism agent also underscores the need for further intervention
572 strategies (114). Periplasmic SOD from *B. abortus,* a major cause of brucellosis, was identified
573 as a major cattle serum-reactive protein that might serve as a *Brucella* vaccine immunogen (16,
574 48, 54). Vaccination with attenuated SOD-deletion strains of *B. abortus* prevented abortion in
575 cattle (115), and vaccination with BaSOD-overexpressing bacteria (116, 117), liposome-

Accepted Manuscript Posted Online

Journal of Bacteriology

JB

Journal of Bacteriology

576 encapsulated BaSOD or nucleic acid BaSOD vaccines (118, 119) also conferred protective
577 advantage. Previous efforts identified one of three tested peptide immunogens from the BaSOD
578 sequence as protective when administered in mice (48). Comparative high-resolution structural
579 analyses of pathogen vs. host proteins enable identification of peptides that promote
580 immunogenicity against pathogens, while minimizing production of host autoantibodies (Fig.
581 S7), a major impetus for this work.

582 **Antigenic targets from new structures.** Our structures provide direct insights for potential
583 peptide-based vaccination efforts against both *N. meningitidis* and *B. abortus*. These P-class
584 SODs contain protruding surface-exposed loops that include insertions relative to E-class SODs
585 (Fig. 6C). Immunogenic peptide BaSOD A56-A67 (48) represents part of such a loop (Fig. S7).
586 Extending this peptide to N52-A67 (and by analogy NmSOD N83-G98) to incorporate the entire
587 loop exposed in bacterial SODs, but buried in the mammalian E-class dimer interface, might
588 elicit an improved response. BaSOD K6-K17 (equivalent to NmSOD K37-K48) represents
589 another such loop. Lastly, the C-terminal NmSOD sequence implicated in HD1 binding might
590 provide another immunogen (Fig. S6), as it also is exposed in P-class SODs, but buried in the E-
591 class dimer interface. The flexibility inherent in these sequences (Fig. 6B and Fig. S2) is
592 important for the interactions of antibody complementarity-determining regions and protein
593 epitopes (120-122). However, to maintain appropriate secondary structure, peptide immunogens
594 may benefit from structural restraints, designed based on hydrogen-bonding, loop conformations,
595 and attachment to the parent protein, as revealed by our NmSOD and BaSOD structures.

596 **Conclusions.** The still-evolving vaccination programs and suboptimal treatments against *N.*
597 *meningitidis* and *B. abortus* (34, 123) underscore the need for novel, additional approaches to
598 intervene in pathogenesis, especially given the emergence of antibiotic resistance. Vaccine and

Accepted Manuscript Posted Online

drug design strategies directed at periplasmic SOD virulence factors (124) benefit from detailed knowledge of structures, assemblies and mechanisms of SODs from bacteria and their hosts. Both microbial and eukaryotic SODs function as master regulators of ROS and can contribute to human disease. In HsSOD ALS mutants, Cu deficiency and flexibility are associated with mis-assembly, aggregation and clinical severity (55). Here, we show that SODs of pathogenic bacteria differ from SODs of their hosts by several targetable means: distinct assembly states, flexible insertions and, sometimes, auxiliary Cu sites that enhance stability. This work provides a framework for predictive understanding of SODs from sequence, highlights similarities and differences between bacterial and eukaryotic enzymes, and describes notable determinants of virulence, which can serve as therapeutic targets.

ACKNOWLEDGMENTS

This work was funded by NIH grant R01GM039345 (to E.D.G. and J.A.T.). Work in the Kroll laboratory was supported by The George John and Sheilah Livanos Charitable Trust. A.J.P. was supported in part through predoctoral NSF and Skaggs Institute for Chemical Biology fellowships and a NIH T32AG000266 postdoctoral training grant. M.D. was supported by a Canadian Institutes of Health Research postdoctoral fellowship. The contributions and technical assistance provided by Chiharu Hitomi, Andrew S. Arvai, Carey Kassman and Zhujin Cao are greatly appreciated. We thank the beamline staff at the Stanford Synchrotron Radiation Laboratory (SSRL) for their help during data collection, and the Structurally-Integrated BiologY for Life Sciences (SIBYLS) beamline at the Advanced Light Source at Lawrence Berkeley National Laboratory. The SIBYLS beamline (BL12.3.1) is funded through the Integrated Diffraction Analysis Technologies (IDAT) program supported by the Department of Energy and

Journal of Bacteriology JB Journal of Bacteriology

Accepted Manuscript Posted Online

622 by NIH grant R01GM105404. Pulse radiolysis studies were carried out at the Center for
623 Radiation Chemical Research, Brookhaven National Laboratory, which was supported under
624 contract DE-AC02-98CH10886 with the U.S. Department of Energy and supported by its
625 Division of Chemical Sciences, Office of Basic Energy Sciences.

626

627

Journal of Bacteriology JB Journal of Bacteriology

Accepted Manuscript Posted Online

Journal of Bacteriology

JB

Journal of Bacteriology

REFERENCES

1. **Perry JJP, Fan L, Tainer JA.** 2007. Developing master keys to brain pathology, cancer and aging from the structural biology of proteins controlling reactive oxygen species and DNA repair. Neuroscience **145:**1280-1299.
2. **Chandel NS, Budinger GR.** 2013. The good and the bad of antibiotics. Sci Transl Med **5:**192fs125.
3. **Imlay JA.** 2013. The molecular mechanisms and physiological consequences of oxidative stress: lessons from a model bacterium. Nat Rev Microbiol **11:**443-454.
4. **Winterbourn CC.** 2008. Reconciling the chemistry and biology of reactive oxygen species. Nat Chem Biol **4:**278-286.
5. **Sena LA, Chandel NS.** 2012. Physiological roles of mitochondrial reactive oxygen species. Mol Cell **48:**158-167.
6. **Fujikawa M, Kobayashi K, Kozawa T.** 2012. Direct oxidation of the [2Fe-2S] cluster in SoxR protein by superoxide: distinct differential sensitivity to superoxide-mediated signal transduction. J Biol Chem **287:**35702-35708.
7. **Green J, Paget MS.** 2004. Bacterial redox sensors. Nat Rev Microbiol **2:**954-966.
8. **Ohsawa T, Tsukahara K, Sato T, Ogura M.** 2006. Superoxide stress decreases expression of srfA through inhibition of transcription of the comQXP quorum-sensing locus in Bacillus subtilis. J Biochem **139:**203-211.
9. **Fridovich I.** 1986. Superoxide dismutases. Adv Enzymol Relat Areas Mol Biol **58:**61-97.
10. **Perry JJ, Shin DS, Getzoff ED, Tainer JA.** 2010. The structural biochemistry of the superoxide dismutases. Biochim Biophys Acta **1804:**245-262.

Accepted Manuscript Posted Online

11. **Shin DS, Didonato M, Barondeau DP, Hura GL, Hitomi C, Berglund JA, Getzoff ED, Cary SC, Tainer JA.** 2009. Superoxide dismutase from the eukaryotic thermophile Alvinella pompejana: structures, stability, mechanism, and insights into amyotrophic lateral sclerosis. J Mol Biol **385:**1534-1555.

12. **Parge HE, Hallewell RA, Tainer JA.** 1992. Atomic structures of wild-type and thermostable mutant recombinant human Cu,Zn superoxide dismutase. Proc Natl Acad Sci U S A **89:**6109-6113.

13. **Tainer JA, Getzoff ED, Beem KM, Richardson JS, Richardson DC.** 1982. Determination and analysis of the 2-Å structure of copper, zinc superoxide dismutase. J Mol Biol **160:**181-217.

14. **Kroll JS, Langford PR, Wilks KE, Keil AD.** 1995. Bacterial [Cu,Zn]-superoxide dismutase: phylogenetically distinct from the eukaryotic enzyme, and not so rare after all! Microbiology **141:**2271-2279.

15. **Imlay KR, Imlay JA.** 1996. Cloning and analysis of *sodC*, encoding the copper-zinc superoxide dismutase of *Escherichia coli*. J Bacteriol **178:**2564-2571.

16. **Beck BL, Tabatabai LB, Mayfield JE.** 1990. A protein isolated from *Brucella abortus* is a Cu-Zn superoxide dismutase. Biochemistry **29:**372-376.

17. **Antonyuk SV, Strange RW, Marklund SL, Hasnain SS.** 2009. The structure of human extracellular copper-zinc superoxide dismutase at 1.7 angstrom resolution: Insights into heparin and collagen binding. J Mol Biol **388:**310-326.

18. **Getzoff ED, Cabelli DE, Fisher CL, Parge HE, Viezzoli MS, Banci L, Hallewell RA.** 1992. Faster superoxide dismutase mutants designed by enhancing electrostatic guidance. Nature **358:**347-351.

Journal of Bacteriology JB Journal of Bacteriology

Accepted Manuscript Posted Online

19. **Bourne Y, Redford SM, Steinman HM, Lepock JR, Tainer JA, Getzoff ED.** 1996. Novel dimeric interface and electrostatic recognition in bacterial Cu,Zn superoxide dismutase. Proc Natl Acad Sci U S A **93:**12774-12779.

20. **Fisher CL, Cabelli DE, Tainer JA, Hallewell RA, Getzoff ED.** 1994. The role of arginine 143 in the electrostatics and mechanism of Cu,Zn superoxide dismutase: computational and experimental evaluation by mutational analysis. Proteins **19:**24-34.

21. **Getzoff ED, Tainer JA, Weiner PK, Kollman PA, Richardson JS, Richardson DC.** 1983. Electrostatic recognition between superoxide and copper, zinc superoxide dismutase. Nature **306:**287-290.

22. **Tainer JA, Getzoff ED, Richardson JS, Richardson DC.** 1983. Structure and mechanism of copper, zinc superoxide dismutase. Nature **306:**284-287.

23. **Stephens DS.** 2007. Conquering the meningococcus. FEMS Microbiol Rev **31:**3-14.

24. **Gomes MT, Campos PC, de Almeida LA, Oliveira FS, Costa MM, Marim FM, Pereira GS, Oliveira SC.** 2012. The role of innate immune signals in immunity to *Brucella abortus*. Front Cell Infect Microbiol **2:**130.

25. **Diacovich L, Gorvel JP.** 2010. Bacterial manipulation of innate immunity to promote infection. Nat Rev Microbiol **8:**117-128.

26. **Rouphael NG, Stephens DS.** 2012. *Neisseria meningitidis*: biology, microbiology, and epidemiology. Methods Mol Biol **799:**1-20.

27. **Caugant DA, Maiden MC.** 2009. Meningococcal carriage and disease--population biology and evolution. Vaccine **27 Suppl 2:**B64-70.

Journal of Bacteriology JB Journal of Bacteriology

Accepted Manuscript Posted Online

28. **Halperin SA, Bettinger JA, Greenwood B, Harrison LH, Jelfs J, Ladhani SN, McIntyre P, Ramsay ME, Safadi MA.** 2012. The changing and dynamic epidemiology of meningococcal disease. Vaccine **30 Suppl 2:**B26-36.

29. **Tan YC, Gill AK, Kim KS.** 2015. Treatment strategies for central nervous system infections: an update. Expert Opin Pharmacother **16:**187-203.

30. **Pappas G, Papadimitriou P, Akritidis N, Christou L, Tsianos EV.** 2006. The new global map of human brucellosis. Lancet Infect Dis **6:**91-99.

31. **Dean AS, Crump L, Greter H, Hattendorf J, Schelling E, Zinsstag J.** 2012. Clinical manifestations of human brucellosis: a systematic review and meta-analysis. PLoS Negl Trop Dis **6:**e1929.

32. **Andrews SM, Pollard AJ.** 2014. A vaccine against serogroup B *Neisseria meningitidis*: dealing with uncertainty. Lancet Infect Dis **14:**426-434.

33. **Avila-Calderon ED, Lopez-Merino A, Sriranganathan N, Boyle SM, Contreras-Rodriguez A.** 2013. A history of the development of Brucella vaccines. Biomed Res Int **2013:**743509.

34. **Yang X, Skyberg JA, Cao L, Clapp B, Thornburg T, Pascual DW.** 2013. Progress in *Brucella* vaccine development. Front Biol (Beijing) **8:**60-77.

35. **Perkins SD, Smither SJ, Atkins HS.** 2010. Towards a *Brucella* vaccine for humans. FEMS Microbiol Rev **34:**379-394.

36. **Craig M, Slauch JM.** 2009. Phagocytic superoxide specifically damages an extracytoplasmic target to inhibit or kill Salmonella. PLoS One **4:**e4975.

37. **Korshunov S, Imlay JA.** 2006. Detection and quantification of superoxide formed within the periplasm of Escherichia coli. J Bacteriol **188:**6326-6334.

Journal of Bacteriology JB Journal of Bacteriology

Accepted Manuscript Posted Online

718 38. **Slauch JM.** 2011. How does the oxidative burst of macrophages kill bacteria? Still an
719 open question. Mol Microbiol **80:**580-583.
720 39. **Ammendola S, Ajello M, Pasquali P, Kroll JS, Langford PR, Rotilio G, Valenti P,**
721 **Battistoni A.** 2005. Differential contribution of *sodC1* and *sodC2* to intracellular survival
722 and pathogenicity of *Salmonella enterica* serovar Choleraesuis. Microbes Infect **7:**698-
723 707.
724 40. **De Groote MA, Ochsner UA, Shiloh MU, Nathan C, McCord JM, Dinauer MC,**
725 **Libby SJ, Vazquez-Torres A, Xu Y, Fang FC.** 1997. Periplasmic superoxide dismutase
726 protects *Salmonella* from products of phagocyte NADPH-oxidase and nitric oxide
727 synthase. Proc Natl Acad Sci U S A **94:**13997-14001.
728 41. **Fang FC, DeGroote MA, Foster JW, Baumler AJ, Ochsner U, Testerman T,**
729 **Bearson S, Giard JC, Xu Y, Campbell G, Laessig T.** 1999. Virulent *Salmonella*
730 *typhimurium* has two periplasmic Cu, Zn-superoxide dismutases. Proc Natl Acad Sci U S
731 A **96:**7502-7507.
732 42. **Melillo AA, Mahawar M, Sellati TJ, Malik M, Metzger DW, Melendez JA, Bakshi**
733 **CS.** 2009. Identification of *Francisella tularensis* live vaccine strain Cu,Zn superoxide
734 dismutase as critical for resistance to extracellularly generated reactive oxygen species. J
735 Bacteriol **191:**6447-6456.
736 43. **Sheehan BJ, Langford PR, Rycroft AN, Kroll JS.** 2000. [Cu,Zn]-Superoxide
737 dismutase mutants of the swine pathogen Actinobacillus pleuropneumoniae are
738 unattenuated in infections of the natural host. Infect Immun **68:**4778-4781.

Journal of Bacteriology
JB
Journal of Bacteriology

Accepted Manuscript Posted Online

739 44. **Wilks KE, Dunn KL, Farrant JL, Reddin KM, Gorringe AR, Langford PR, Kroll**
740 **JS.** 1998. Periplasmic superoxide dismutase in meningococcal pathogenicity. Infect
741 Immun **66:**213-217.
742 45. **Dunn KLR, Farrant JL, Langford PR, Kroll JS.** 2003. Bacterial [Cu,Zn]-cofactored
743 superoxide dismutase protects opsonized, encapsulated *Neisseria meningitidis* from
744 phagocytosis by human monocytes/macrophages. Infect Immun **71:**1604-1607.
745 46. **Gee JM, Valderas MW, Kovach ME, Grippe VK, Robertson GT, Ng WL,**
746 **Richardson JM, Winkler ME, Roop RM.** 2005. The *Brucella abortus* Cu,Zn
747 superoxide dismutase is required for optimal resistance to oxidative killing by murine
748 macrophages and wild-type virulence in experimentally infected mice. Infect Immun
749 **73:**2873-2880.
750 47. **Tatum FM, Detilleux PG, Sacks JM, Halling SM.** 1992. Construction of Cu-Zn
751 superoxide dismutase deletion mutants of *Brucella abortus*: analysis of survival in vitro
752 in epithelial and phagocytic cells and in vivo in mice. Infect Immun **60:**2863-2869.
753 48. **Tabatabai LB, Pugh GW, Jr.** 1994. Modulation of immune responses in Balb/c mice
754 vaccinated with *Brucella abortus* Cu-Zn superoxide dismutase synthetic peptide vaccine.
755 Vaccine **12:**919-924.
756 49. **Fung WW, O'Dwyer CA, Sinha S, Brauer AL, Murphy TF, Kroll JS, Langford PR.**
757 2006. Presence of copper- and zinc-containing superoxide dismutase in commensal
758 *Haemophilus haemolyticus* isolates can be used as a marker to discriminate them from
759 nontypeable *H. influenzae* isolates. J Clin Microbiol **44:**4222-4226.
760 50. **Putnam CD, Hammel M, Hura GL, Tainer JA.** 2007. X-ray solution scattering
761 (SAXS) combined with crystallography and computation: defining accurate

Journal of Bacteriology
JB
Journal of Bacteriology

Accepted Manuscript Posted Online

762 macromolecular structures, conformations and assemblies in solution. Q Rev Biophys
763 **40:**191-285.

764 51. **Natvig DO, Imlay K, Touati D, Hallewell RA.** 1987. Human copper-zinc superoxide
765 dismutase complements superoxide dismutase-deficient *Escherichia coli* mutants. J Biol
766 Chem **262:**14697-14701.

767 52. **Boissinot M, Karnas S, Lepock JR, Cabelli DE, Tainer JA, Getzoff ED, Hallewell**
768 **RA.** 1997. Function of the Greek key connection analysed using circular permutants of
769 superoxide dismutase. EMBO J **16:**2171-2178.

770 53. **Chen YL, Park S, Thornburg RW, Tabatabai LB, Kintanar A.** 1995. Structural
771 characterization of the active site of *Brucella abortus* Cu-Zn superoxide dismutase: a 15N
772 and 1H NMR investigation. Biochemistry **34:**12265-12275.

773 54. **Bricker BJ, Tabatabai LB, Judge BA, Deyoe BL, Mayfield JE.** 1990. Cloning,
774 expression, and occurrence of the *Brucella* Cu-Zn superoxide dismutase. Infect Immun
775 **58:**2935-2939.

776 55. **Pratt AJ, Shin DS, Merz GE, Rambo RP, Lancaster WA, Dyer KN, Borbat PP,**
777 **Poole FL, 2nd, Adams MW, Freed JH, Crane BR, Tainer JA, Getzoff ED.** 2014.
778 Aggregation propensities of superoxide dismutase G93 hotspot mutants mirror ALS
779 clinical phenotypes. Proc Natl Acad Sci U S A **111:**E4568-4576.

780 56. **DiDonato M, Craig L, Huff ME, Thayer MM, Cardoso RM, Kassmann CJ, Lo TP,**
781 **Bruns CK, Powers ET, Kelly JW, Getzoff ED, Tainer JA.** 2003. ALS mutants of
782 human superoxide dismutase form fibrous aggregates via framework destabilization. J
783 Mol Biol **332:**601-615.

784 57. **Flohe L, Otting F.** 1984. Superoxide dismutase assays. Methods Enzymol **105:**93-104.

Journal of Bacteriology
JB
Journal of Bacteriology

Accepted Manuscript Posted Online

785 58. **Navaza J.** 1994. AMoRe: an automated package for molecular replacement. Acta
786 Crystallogr A **50:**157-163.
787 59. **Brünger AT, Adams PD, Clore GM, DeLano WL, Gros P, Grosse-Kunstleve RW,**
788 **Jiang J-S, Kuszewski J, Nilges M, Pannu NS, Read RJ, Rice LM, Simonson T,**
789 **Warren GL.** 1998. Crystallography & NMR system: a new software suite for
790 macromolecular structure determination. Acta Crystallogr D Biol Crystallogr **54:**905-
791 921.
792 60. **McRee DE.** 1999. XtalView/Xfit - A versatile program for manipulating atomic
793 coordinates and electron density. J Struct Biol **125:**156-165.
794 61. **Sheldrick GM, Schneider TR.** 1997. SHELXL: High-Resolution Refinement. Methods
795 Enzymol **277:**319-343.
796 62. **Adams PD, Afonine PV, Bunkoczi G, Chen VB, Davis IW, Echols N, Headd JJ,**
797 **Hung LW, Kapral GJ, Grosse-Kunstleve RW, McCoy AJ, Moriarty NW, Oeffner R,**
798 **Read RJ, Richardson DC, Richardson JS, Terwilliger TC, Zwart PH.** 2010.
799 PHENIX: a comprehensive Python-based system for macromolecular structure solution.
800 Acta Crystallographica Section D-Biological Crystallography **66:**213-221.
801 63. **Classen S, Hura GL, Holton JM, Rambo RP, Rodic I, McGuire PJ, Dyer K,**
802 **Hammel M, Meigs G, Frankel KA, Tainer JA.** 2013. Implementation and performance
803 of SIBYLS: a dual endstation small-angle X-ray scattering and macromolecular
804 crystallography beamline at the Advanced Light Source. J Appl Crystallogr **46:**1-13.
805 64. **Konarev PV, Volkov VV, Sokolova AV, Koch MHJ, Svergun DI.** 2003. PRIMUS: a
806 Windows PC-based system for small-angle scattering data analysis. J Appl Crystallogr
807 **36:**1277-1282.

Journal of Bacteriology
JB
Journal of Bacteriology

Accepted Manuscript Posted Online

65. **Semenyuk AV, Svergun DI.** 1991. Gnom - a program package for small-angle scattering data-processing. J Appl Crystallogr **24:**537-540.

66. **Franke D, Svergun DI.** 2009. DAMMIF, a program for rapid ab-initio shape determination in small-angle scattering. J Appl Cryst **42:**342-346.

67. **Volkov VV, Svergun DI.** 2003. Uniqueness of ab initio shape determination in small-angle scattering. J Appl Crystallogr **36:**860-864.

68. **Schneidman-Duhovny D, Hammel M, Sali A.** 2010. FoXS: a web server for rapid computation and fitting of SAXS profiles. Nucleic Acids Res **38:**W540-544.

69. **Pettersen EF, Goddard TD, Huang CC, Couch GS, Greenblatt DM, Meng EC, Ferrin TE.** 2004. UCSF Chimera--a visualization system for exploratory research and analysis. J Comput Chem **25:**1605-1612.

70. **Suhre K, Sanejouand YH.** 2004. ElNemo: a normal mode web server for protein movement analysis and the generation of templates for molecular replacement. Nucleic Acids Res **32:**W610-614.

71. **Battistoni A, Pacello F, Mazzetti AP, Capo C, Kroll JS, Langford PR, Sansone A, Donnarumma G, Valenti P, Rotilio G.** 2001. A histidine-rich metal binding domain at the N terminus of Cu,Zn-superoxide dismutases from pathogenic bacteria. J Biol Chem **276:**30315-30325.

72. **(CDC). CfDCaP.** 2013. Updated recommendations for use of VariZIG--United States, 2013. MMWR Morb Mortal Wkly Rep **62:**574-576.

73. **Blaise A, Gautret P.** 2015. Current perspectives on rabies postexposure prophylaxis. Infect Disord Drug Targets **15:**13-19.

Journal of Bacteriology JB Journal of Bacteriology

Accepted Manuscript Posted Online

74. **Forest KT, Langford PR, Kroll JS, Getzoff ED.** 2000. Cu,Zn superoxide dismutase structure from a microbial pathogen establishes a class with a conserved dimer interface. J Mol Biol **296:**145-153.

75. **Toro I, Petrutz C, Pacello F, D'Orazio M, Battistoni A, Djinovic-Carugo K.** 2009. Structural basis of heme binding in the Cu,Zn superoxide dismutase from *Haemophilus ducreyi*. J Mol Biol **386:**406-418.

76. **Bordo D, Matak D, Djinovic-Carugo K, Rosano C, Pesce A, Bolognesi M, Stroppolo ME, Falconi M, Battistoni A, Desideri A.** 1999. Evolutionary constraints for dimer formation in prokaryotic Cu,Zn superoxide dismutase. J Mol Biol **285:**283-296.

77. **Cioni P, Pesce A, Morozzo della Rocca B, Castelli S, Falconi M, Parrilli L, Bolognesi M, Strambini G, Desideri A.** 2003. Active-site copper and zinc ions modulate the quaternary structure of prokaryotic Cu,Zn superoxide dismutase. J Mol Biol **326:**1351-1360.

78. **Pesce A, Battistoni A, Stroppolo ME, Polizio F, Nardini M, Kroll JS, Langford PR, O'Neill P, Sette M, Desideri A, Bolognesi M.** 2000. Functional and crystallographic characterization of *Salmonella typhimurium* Cu,Zn superoxide dismutase coded by the *sodCI* virulence gene. J Mol Biol **302:**465-478.

79. **Hura GL, Budworth H, Dyer KN, Rambo RP, Hammel M, McMurray CT, Tainer JA.** 2013. Comprehensive macromolecular conformations mapped by quantitative SAXS analyses. Nat Methods **10:**453-454.

80. **Rambo RP, Tainer JA.** 2013. Accurate assessment of mass, models and resolution by small-angle scattering. Nature **496:**477-481.

Journal of Bacteriology JB Journal of Bacteriology

Accepted Manuscript Posted Online

852 81. **Rambo RP, Tainer JA.** 2011. Characterizing flexible and intrinsically unstructured
853 biological macromolecules by SAS using the Porod-Debye law. Biopolymers **95:**559-
854 571.
855 82. **Ogihara NL, Parge HE, Hart PJ, Weiss MS, Goto JJ, Crane BR, Tsang J, Slater K,**
856 **Roe JA, Valentine JS, Eisenberg D, Tainer JA.** 1996. Unusual trigonal-planar copper
857 configuration revealed in the atomic structure of yeast copper-zinc superoxide dismutase.
858 Biochemistry **35:**2316-2321.
859 83. **Folcarelli S, Battistoni A, Falconi M, O'Neill P, Rotilio G, Desideri A.** 1998.
860 Conserved enzyme-substrate electrostatic attraction in prokaryotic Cu,Zn superoxide
861 dismutases. Biochem Biophys Res Commun **244:**908-911.
862 84. **Pacello F, Langford PR, Kroll JS, Indiani C, Smulevich G, Desideri A, Rotilio G,**
863 **Battistoni A.** 2001. A novel heme protein, the Cu,Zn-superoxide dismutase from
864 *Haemophilus ducreyi*. J Biol Chem **276:**30326-30334.
865 85. **Tainer JA, Roberts VA, Fisher CL, Hallewell RA, Getzoff ED.** 1991. Mechanism and
866 Structure of Superoxide Dismutases. *In* Kuby SA (ed), A Study of Enzymes II
867 Mechanism of Enzyme Action. CRC, Boca Raton, FL.
868 86. **Pesce A, Capasso C, Battistoni A, Folcarelli S, Rotilio G, Desideri A, Bolognesi M.**
869 1997. Unique structural features of the monomeric Cu,Zn superoxide dismutase from
870 *Escherichia coli*, revealed by X-ray crystallography. J Mol Biol **274:**408-420.
871 87. **Mori M, Jimenez B, Piccioli M, Battistoni A, Sette M.** 2008. The Solution Structure of
872 the Monomeric Copper, Zinc Superoxide Dismutase from *Salmonella enterica:* Structural
873 Insights To Understand the Evolution toward the Dimeric Structure. Biochemistry
874 **47:**12954-12963.

Journal of Bacteriology
JB
Journal of Bacteriology

Accepted Manuscript Posted Online

875 88. **Banci L, Bertini I, Calderone V, Cramaro F, Del Conte R, Fantoni A, Mangani S,**
876 **Quattrone A, Viezzoli MS.** 2005. A prokaryotic superoxide dismutase paralog lacking
877 two Cu ligands: from largely unstructured in solution to ordered in the crystal. Proc Natl
878 Acad Sci U S A **102:**7541-7546.
879 89. **Hallewell RA, Laria I, Tabrizi A, Carlin G, Getzoff ED, Tainer JA, Cousens LS,**
880 **Mullenbach GT.** 1989. Genetically engineered polymers of human Cu,Zn superoxide-
881 dismutase - Biochemistry and serum half-lives. J Biol Chem **264:**5260-5268.
882 90. **Spagnolo L, Toro I, D'Orazio M, O'Neill P, Pedersen JZ, Carugo O, Rotilio G,**
883 **Battistoni A, Djinovic-Carugo K.** 2004. Unique features of the *sodC*-encoded
884 superoxide dismutase from *Mycobacterium tuberculosis*, a fully functional copper-
885 containing enzyme lacking zinc in the active site. J Biol Chem **279:**33447-33455.
886 91. **Gleason JE, Galaleldeen A, Peterson RL, Taylor AB, Holloway SP, Waninger-**
887 **Saroni J, Cormack BP, Cabelli DE, Hart PJ, Culotta VC.** 2014. *Candida albicans*
888 SOD5 represents the prototype of an unprecedented class of Cu-only superoxide
889 dismutases required for pathogen defense. Proc Natl Acad Sci U S A **111:**5866-5871.
890 92. **Elam JS, Taylor AB, Strange R, Antonyuk S, Doucette PA, Rodriguez JA, Hasnain**
891 **SS, Hayward LJ, Valentine JS, Yeates TO, Hart PJ.** 2003. Amyloid-like filaments and
892 water-filled nanotubes formed by SOD1 mutant proteins linked to familial ALS. Nat
893 Struct Biol **10:**461-467.
894 93. **Rambo RP, Tainer JA.** 2013. Super-resolution in solution X-ray scattering and its
895 applications to structural systems biology. Annu Rev Biophys **42:**415-441.
896 94. **Hura GL, Menon AL, Hammel M, Rambo RP, Poole FL, 2nd, Tsutakawa SE,**
897 **Jenney FE, Jr., Classen S, Frankel KA, Hopkins RC, Yang SJ, Scott JW, Dillard**

Journal of Bacteriology
JB
Journal of Bacteriology

Accepted Manuscript Posted Online

898 **BD, Adams MW, Tainer JA.** 2009. Robust, high-throughput solution structural analyses
899 by small angle X-ray scattering (SAXS). Nat Methods **6:**606-612.
900 95. **McRee DE, Redford SM, Getzoff ED, Lepock JR, Hallewell RA, Tainer JA.** 1990.
901 Changes in crystallographic structure and thermostability of a Cu,Zn superoxide
902 dismutase mutant resulting from the removal of a buried cysteine. J Biol Chem
903 **265:**14234-14241.
904 96. **Kadokura H, Beckwith J.** 2010. Mechanisms of oxidative protein folding in the
905 bacterial cell envelope. Antioxid Redox Signal **13:**1231-1246.
906 97. **Dutton RJ, Boyd D, Berkmen M, Beckwith J.** 2008. Bacterial species exhibit diversity
907 in their mechanisms and capacity for protein disulfide bond formation. Proc Natl Acad
908 Sci U S A **105:**11933-11938.
909 98. **Getzoff ED, Tainer JA, Stempien MM, Bell GI, Hallewell RA.** 1989. Evolution of
910 CuZn superoxide dismutase and the Greek key beta-barrel structural motif. Proteins
911 **5:**322-336.
912 99. **Rushing MD, Slauch JM.** 2011. Either periplasmic tethering or protease resistance is
913 sufficient to allow a SodC to protect Salmonella enterica serovar Typhimurium from
914 phagocytic superoxide. Mol Microbiol **82:**952-963.
915 100. **Kang M, Duncan GA, Kuszynski C, Oyler G, Zheng J, Becker DF, Van Etten JL.**
916 2015. Chlorovirus *PBCV-1* encodes an active copper-zinc superoxide dismutase. J Virol
917 **88:**12541-12550.
918 101. **Lartigue A, Burlat B, Coutard B, Chaspoul F, Claverie JM, Abergel C.** 2015. The
919 megavirus chilensis Cu,Zn-superoxide dismutase: the first viral structure of a typical
920 cellular copper chaperone-independent hyperstable dimeric enzyme. J Virol **89:**824-832.

Journal of Bacteriology
JB
Journal of Bacteriology

Accepted Manuscript Posted Online

921 102. **Mullenbach GT, Tabrizi A, Irvine BD, Bell GI, Tainer JA, Hallewell RA.** 1988.
922 Selenocysteines mechanism of incorporation and evolution revealed in cDNAs of 3
923 glutathione peroxidases. Protein Eng **2:**239-246.
924 103. **Dupont CL, Butcher A, Valas RE, Bourne PE, Caetano-Anolles G.** 2010. History of
925 biological metal utilization inferred through phylogenomic analysis of protein structures.
926 Proc Natl Acad Sci U S A **107:**10567-10572.
927 104. **Festa RA, Thiele DJ.** 2012. Copper at the front line of the host-pathogen battle. PLoS
928 Pathog **8:**e1002887.
929 105. **Kadiiska MB, Mason RP.** 2002. In vivo copper-mediated free radical production: an
930 ESR spin-trapping study. Spectrochim Acta A Mol Biomol Spectrosc **58:**1227-1239.
931 106. **D'angelo P, Pacello F, Mancini G, Proux O, Hazemann JL, Desideri A, Battistoni A.**
932 2005. X-ray absorption investigation of a unique protein domain able to bind both
933 copper(I) and copper(II) at adjacent sites of the N-terminus of *Haemophilus ducreyi*
934 Cu,Zn superoxide dismutase. Biochemistry **44:**13144-13150.
935 107. **Arus D, Jancso A, Szunyogh D, Matyuska F, Nagy NV, Hoffmann E, Kortvelyesi T,**
936 **Gajda T.** 2012. On the possible roles of N-terminal His-rich domains of Cu,Zn SODs of
937 some Gram-negative bacteria. J Inorg Biochem **106:**10-18.
938 108. **Cun SJ, Li HY, Ge RG, Lin MCM, Sun HZ.** 2008. A histidine-rich and cysteine-rich
939 metal-binding domain at the C terminus of heat shock protein A from *Helicobacter pylori*
940 - Implication for nickel homeostasis and bismuth susceptibility. J Biol Chem **283:**15142-
941 15151.
942 109. **Cvetkovic A, Menon AL, Thorgersen MP, Scott JW, Poole FL, Jenney FE,**
943 **Lancaster WA, Praissman JL, Shanmukh S, Vaccaro BJ, Trauger SA, Kalisiak E,**

Journal of Bacteriology
JB
Journal of Bacteriology

Accepted Manuscript Posted Online

944 **Apon JV, Siuzdak G, Yannone SM, Tainer JA, Adams MWW.** 2010. Microbial
945 metalloproteomes are largely uncharacterized. Nature **466:**779-U718.
946 110. **Chillemi G, De Santis S, Falconi M, Mancini G, Migliorati V, Battistoni A, Pacello**
947 **F, Desideri A, D'Angelo P.** 2012. Carbon monoxide binding to the heme group at the
948 dimeric interface modulates structure and copper accessibility in the Cu,Zn superoxide
949 dismutase from *Haemophilus ducreyi*: in silico and in vitro evidences. J Biomol Struct
950 Dyn **30:**269-279.
951 111. **Stroppolo ME, Pesce A, D'Orazio M, O'Neill P, Bordo D, Rosano C, Milani M,**
952 **Battistoni A, Bolognesi M, Desideri A.** 2001. Single mutations at the subunit interface
953 modulate copper reactivity in *Photobacterium leiognathi* Cu,Zn superoxide dismutase. J
954 Mol Biol **308:**555-563.
955 112. **Seib KL, Scarselli M, Comanducci M, Toneatto D, Masignani V.** 2015. *Neisseria*
956 *meningitidis* factor H-binding protein fHbp: a key virulence factor and vaccine antigen.
957 Expert Rev Vaccines **14:**841-859.
958 113. **Ashford DA, di Pietra J, Lingappa J, Woods C, Noll H, Neville B, Weyant R, Bragg**
959 **SL, Spiegel RA, Tappero J, Perkins BA.** 2004. Adverse events in humans associated
960 with accidental exposure to the livestock brucellosis vaccine RB51. Vaccine **22:**3435-
961 3439.
962 114. **Doganay GD, Doganay M.** 2013. *Brucella* as a potential agent of bioterrorism. Recent
963 Pat Antiinfect Drug Discov **8:**27-33.
964 115. **Cheville NF, Stevens MG, Jensen AE, Tatum FM, Halling SM.** 1993. Immune
965 responses and protection against infection and abortion in cattle experimentally
966 vaccinated with mutant strains of *Brucella abortus*. Am J Vet Res **54:**1591-1597.

Journal of Bacteriology
JB
Journal of Bacteriology

Accepted Manuscript Posted Online

967 116. **Saez D, Fernandez P, Rivera A, Andrews E, Onate A.** 2012. Oral immunization of
968 mice with recombinant *Lactococcus lactis* expressing Cu,Zn superoxide dismutase of
969 *Brucella abortus* triggers protective immunity. Vaccine **30:**1283-1290.
970 117. **Rajasekaran P, Surendran N, Seleem MN, Sriranganathan N, Schurig GG, Boyle**
971 **SM.** 2011. Over-expression of homologous antigens in a leucine auxotroph of *Brucella*
972 *abortus* strain RB51 protects mice against a virulent *B. suis* challenge. Vaccine **29:**3106-
973 3110.
974 118. **Singha H, Mallick AI, Jana C, Fatima N, Owais M, Chaudhuri P.** 2011. Co-
975 immunization with interleukin-18 enhances the protective efficacy of liposomes
976 encapsulated recombinant Cu-Zn superoxide dismutase protein against *Brucella abortus*.
977 Vaccine **29:**4720-4727.
978 119. **Retamal-Diaz A, Riquelme-Neira R, Saez D, Rivera A, Fernandez P, Cabrera A,**
979 **Guzman CA, Onate A.** 2014. Use of S-[2,3-bispalmitoyiloxy-(2R)-propyl]-R-cysteinyl-
980 amido-monomethoxy polyethylene glycol as an adjuvant improved protective immunity
981 associated with a DNA vaccine encoding Cu,Zn superoxide dismutase of *Brucella*
982 *abortus* in mice. Clin Vaccine Immunol **21:**1474-1480.
983 120. **Tainer JA, Getzoff ED, Alexander H, Houghten RA, Olson AJ, Lerner RA,**
984 **Hendrickson WA.** 1984. The reactivity of anti-peptide antibodies is a function of the
985 atomic mobility of sites in a protein. Nature **312:**127-134.
986 121. **Forest KT, Bernstein SL, Getzoff ED, So M, Tribbick G, Geysen HM, Deal CD,**
987 **Tainer JA.** 1996. Assembly and antigenicity of the *Neisseria gonorrhoeae* pilus mapped
988 with antibodies. Infect Immun **64:**644-652.

Journal of Bacteriology
JB
Journal of Bacteriology

Accepted Manuscript Posted Online

122. **Getzoff ED, Tainer JA, Lerner RA, Geysen HM.** 1988. The chemistry and mechanism of antibody-binding to protein antigens. Adv Immunol **43:**1-98.

123. **van de Beek D, Brouwer MC, Thwaites GE, Tunkel AR.** 2012. Advances in treatment of bacterial meningitis. Lancet **380:**1693-1702.

124. **Beceiro A, Tomas M, Bou G.** 2013. Antimicrobial resistance and virulence: a successful or deleterious association in the bacterial world? Clin Microbiol Rev **26:**185-230.

Journal of Bacteriology JB Journal of Bacteriology

Accepted Manuscript Posted Online

Journal of Bacteriology

JB

998 **FIGURE LEGENDS**

999 **FIG 1** NmSOD-reactive monoclonal antibody HD1 protects mice from *N. meningitidis*
1000 serogroup B infection. Mice were challenged with bacteria co-administered with the antibody
1001 (HD1) or without (control). As indicated by survival data, HD1 conferred passive protection
1002 against experimental infection.

1003

1004 **FIG 2** Three-dimensional X-ray structures of *N. meningitidis* Cu,ZnSOD (NmSOD, gold) and *B.*
1005 *abortus* Cu,ZnSOD (BaSOD, blue). (A) NmSOD is a P-class homodimer of conserved Greek-
1006 key β-barrel SOD subunits (β-strands in gold, α-helices in green). Buried interface water residues
1007 are depicted as red spheres, disulfide positions by S-S and active-site Cu and Zn ions by bronze
1008 and silver spheres, respectively. (B) BaSOD is a monomer with the same conserved SOD fold
1009 (β-strands in blue, α-helices in purple). (C) Close-up of NmSOD (top) and BaSOD (bottom)
1010 active sites with metal-binding histidine and aspartic acid ligand side chains shown and the Cu
1011 ligands labeled. The redox-active Cu site and bridging histidine are modeled in two positions
1012 (oxidized and reduced) in BaSOD. (D) Experimental SAXS data (gold and blue) fit SAXS
1013 profiles (red and black) simulated from the crystallographic assemblies (NmSOD dimer and
1014 BaSOD monomer, respectively). Residuals (experimental/model intensity ratio) are depicted
1015 below profiles. (E) Real-space electron pair distributions for NmSOD and BaSOD reveal
1016 significant differences in overall shape and dimensions of these two enzymes in solution,
1017 consistent with NmSOD P-Class dimer assembly and monomeric BaSOD. (F) X-ray structures
1018 of NmSOD (left) and BaSOD (right) docked into *ab initio* envelopes modeled from SAXS data
1019 show agreement between crystalline and solution X-ray data.

1020

Accepted Manuscript Posted Online

FIG 3 Comparative structural assemblies of SODs and SOD homologs are linked to sequence motifs. (A) Distinct quaternary arrangements of bacterial and eukaryotic Cu,ZnSODs (SODs) and SOD homolog. Top and side views (relative to the β-barrel) depict Cα traces for 4 distinct, representative dimers, superimposed using one reference subunit (red) each: P-class *N. meningitidis* SOD (orange; PDB code: 2AQN), loop class (L-class) *M. tuberculosis* SOD (cyan; PDB code: 1PZS), E-class human SOD (HsSOD, green; PDB code 1PU0) dimers, and crystallographic *B. subtilis* SOD-like dimer (magenta; PDB code: 1S4I), although this homolog is monomeric in solution. For comparison, the buried dimer interface surface areas for SOD homologs were computed with the PISA webserver (http://www.ebi.ac.uk/msd-srv/prot_int/cgi-bin/piserver): NmSOD (915 Å^2), *M. tuberculosis* (1636 Å^2), HsSOD (~704 Å^2) and the *B. subtilis* SOD-like homolog (~347 Å^2). PISA predicts *B. abortus* SOD to be monomeric. However, PISA also predicts the crystallographic BsSOD dimer to be stable. (B) NmSOD dimer structure and surface, bisected at the dimer interface, highlights P-class dimer-specific residues (red), which are located around the perimeter of the water-filled cavity buried in the dimer interface. Red residues correspond to red sequence motifs depicted in part C. Black star denotes position of NmSOD-specific cavity adjacent to auxiliary Cu site (gold sphere). (C) Sequence alignment representing 4 SOD assembly classes: BaSOD (P-class monomer), NmSOD (P-class dimer), *M. tuberculosis* (L-class dimer) and HsSOD (E-class dimer). Bacterial sequences start at the site of signal peptidase cleavage. Conserved sequence motifs (magenta, except where indicated) include the leucine "cork," (replaced by a single residue insertion in fungi) starting the conserved LxxGxHG pattern, Cu ligands (gold H or gold/silver bridging H), Zn ligands (gold/silver bridging H or silver D/H, missing in some L-class SODs), aspartic acid that indirectly bridges Cu and Zn ligands via hydrogen bonds and the Rx(A/V)CGV(I/V) motif (near

Journal of Bacteriology JB Journal of Bacteriology

Accepted Manuscript Posted Online

Journal of Bacteriology

JB

Journal of Bacteriology

1044 C-terminus), which includes both the conserved active-site arginine (italic R) and invariant
1045 second cysteine of conserved disulfide bond. Discriminating features of E-class SODs include:
1046 conserved residues involved in electrostatic guidance (indicated by purple italics), first cysteine
1047 of conserved disulfide bond (light green C) located 6 residues before bridging histidine and an
1048 aromatic or hydrophobic interface residue (yellow F, followed by G) located 2 residues after the
1049 second Cu ligand (Cu2). Discriminating features of bacterial SODs include: distinct residues
1050 implicated in electrostatic guidance (purple italics in boxed sequence), first cysteine of conserved
1051 disulfide bond (green C) located 5 residues after Cu2, an insertion ~7 residues after Cu2 in P-
1052 class SODs, and an insertion ~10 residues after the fourth Cu ligand (Cu4) in L-class SODs.
1053 Discriminating features in P-class dimers, but not monomers (red lettering), include: a semi-
1054 conserved YG motif, located 11 residues N-terminal to the conserved leucine cork; a
1055 hydrophobic residue (typically V or L; V in NmSOD) 8 residues before the leucine cork; a
1056 hydrophobic residue, preceded by glycine, substituted in monomers with a residue capable of
1057 hydrogen-bonding, located ~4 residues after the cork leucine (L in NmSOD); an aromatic
1058 tryptophan or tyrosine in P-class SOD dimers 7-8 residues before conserved aspartate (Zn ligand
1059 in many SODs) substituted to a charged residue in other classes (W in NmSOD). Protective (red
1060 bar) and non-protective (orange bars) peptide immunogens (48) are mapped below the BaSOD
1061 sequence. Approximate position of conserved secondary structural elements are denoted below
1062 sequences as arrows (β-strands) and coils (α-helices). The blue arrows denote P-class secondary
1063 structure in bacterial-specific insertion, and the turquoise coil denotes a L- and P-class-specific
1064 secondary structure feature.
1065
1066 **FIG 4** Role of NmSOD residues in Cu binding and activity. (A) Identification of electrostatic

Accepted Manuscript Posted Online

guidance residues in NmSOD. The reaction rate constant for NmSOD electrostatics mutants as a function of pH was evaluated using pulse radiolysis. Whereas the E73A mutation has no effect on the reaction rate constant, reversing or neutralizing the charge at both proposed electrostatic residues K91 and K94, caused a substantial decrease in the reaction rate constant. (B) NmSOD E73 contributes to protein stability, as assayed by monitoring guanidine-HCl unfolding of WT and E73A NmSOD, and WT HsSOD, with circular dichroism (CD) spectroscopy. The unfolding midpoint for the E73A mutant is approximately 0.6-0.7 M lower than for WT NmSOD. Asterisks denote data points omitted from the fitting. (C) Close-up looking down the two-fold dimer axis of WT NmSOD (top). The E73 and H133 side chains from each subunit of the dimer are positioned with tetrahedral coordination geometry around the Cu ion. Auxiliary Cu binding was abrogated in E73A mutant (bottom), wherein only solvent molecules are observed at the equivalent site. (D) Superposition of NmSOD and heme-bound HdSOD (PDB code: 1Z9P) reveals parallel structure and dimer assembly. (E) Zoom into binding site (dashed box in part D) reveals similarities in Cu binding by NmSOD E73 and H133 as compared to heme binding by HdSOD H64 and H124.

FIG 5 Potential roles of NmSOD auxiliary Cu site. (A) Overview (top) and close-up views (bottom) of binding pocket below NmSOD auxiliary Cu site. Surface rendering suggested pocket volume (124.6 $Å^3$) could accommodate small molecules. (B) Suggested mechanisms for virulence utilized in NmSOD upon phagocytosis. NmSOD counters reactive oxygen species through its dismutase activity and buffers toxic Cu influx through its cross-dimer Cu binding site.

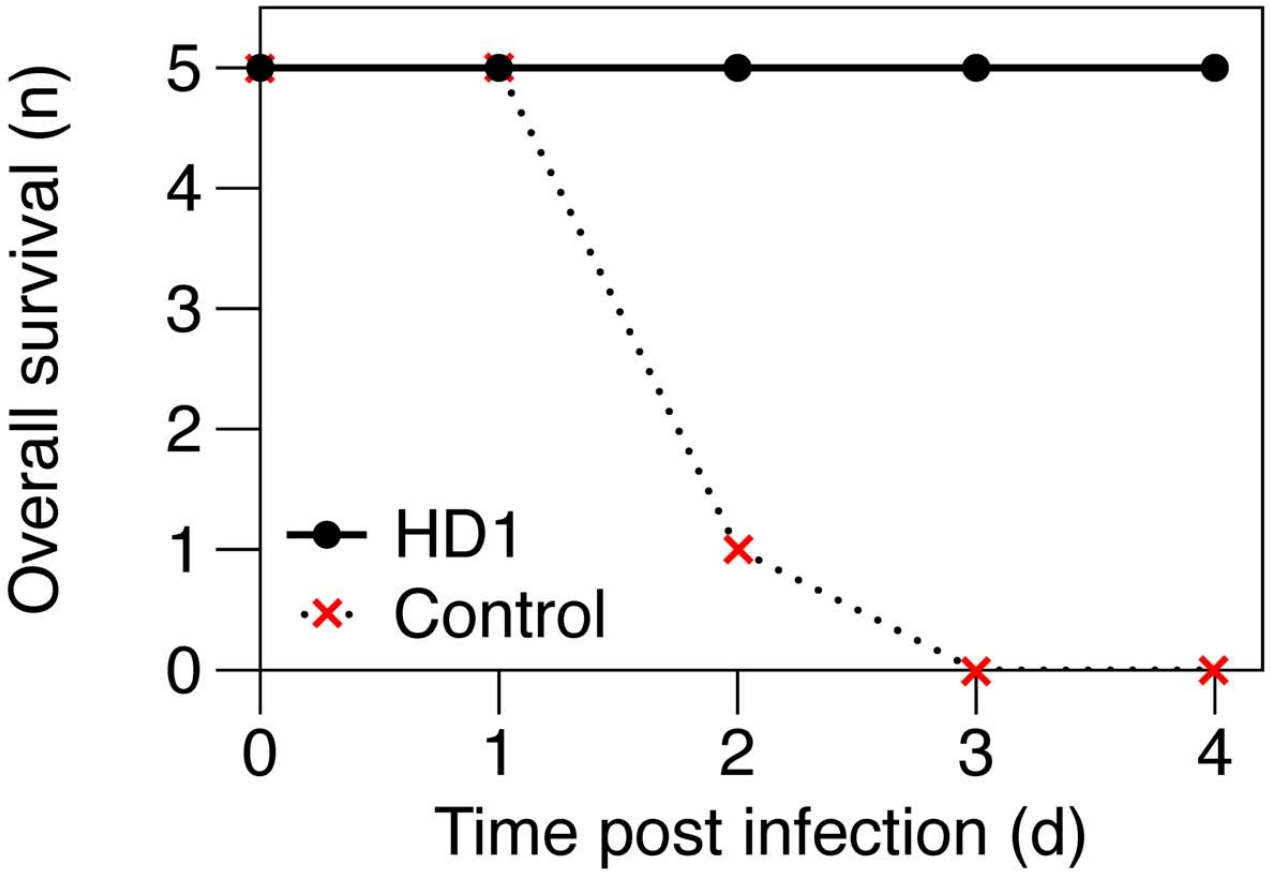
Journal of Bacteriology JB Journal of Bacteriology

Accepted Manuscript Posted Online

1090 **FIG 6** Immunogen extension from new SOD structures. (A) Comparison of NmSOD and
1091 BaSOD with HsSOD. Identical residues (magenta) were mapped onto superposed HsSOD (light
1092 gray) with NmSOD (gold, left) or BaSOD (blue, right) molecular surfaces. Despite the large
1093 evolutionary separation between bacterial and mammalian SODs, BaSOD and NmSOD contain
1094 many residues identical to HsSOD, predominantly near the active site. (B) C_α atomic
1095 displacement parameters (ADP; B-factor) for NmSOD and BaSOD are plotted by residue.
1096 Increased mobility was noted predominantly in two regions specific to bacterial SODs (an
1097 extended loop, green, and a bacterial insertion, red). These two regions were similarly suggested
1098 to be mobile using normal mode analysis. Superimposed normal mode analysis models (from
1099 Fig. S2) are inset in plot for NmSOD (top, gold) and BaSOD (bottom, blue). (C) Superposition
1100 of single subunits from bacterial SOD (NmSOD, gold, left or BaSOD, blue, center) and HsSOD
1101 (gray) crystallographic structures also reveals that the afore-mentioned insertions/loops
1102 characteristic of bacterial SODs are non-conserved regions in 3-dimensional space. These
1103 potential immunogens were mapped onto aligned SOD subunits (right) in red and green.

Journal of Bacteriology
JB
Journal of Bacteriology

Accepted Manuscript Posted Online
Journal of Bacteriology
JB
Journal of Bacteriology

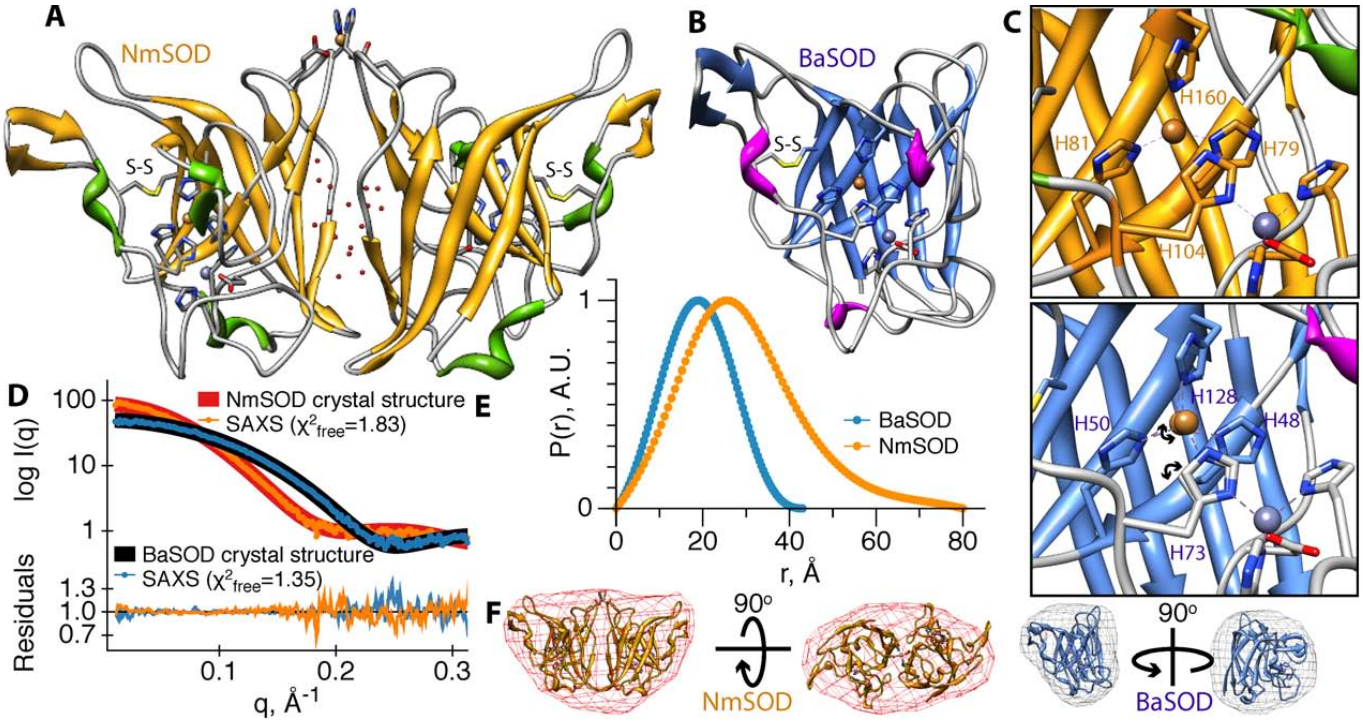


Accepted Manuscript Posted Online

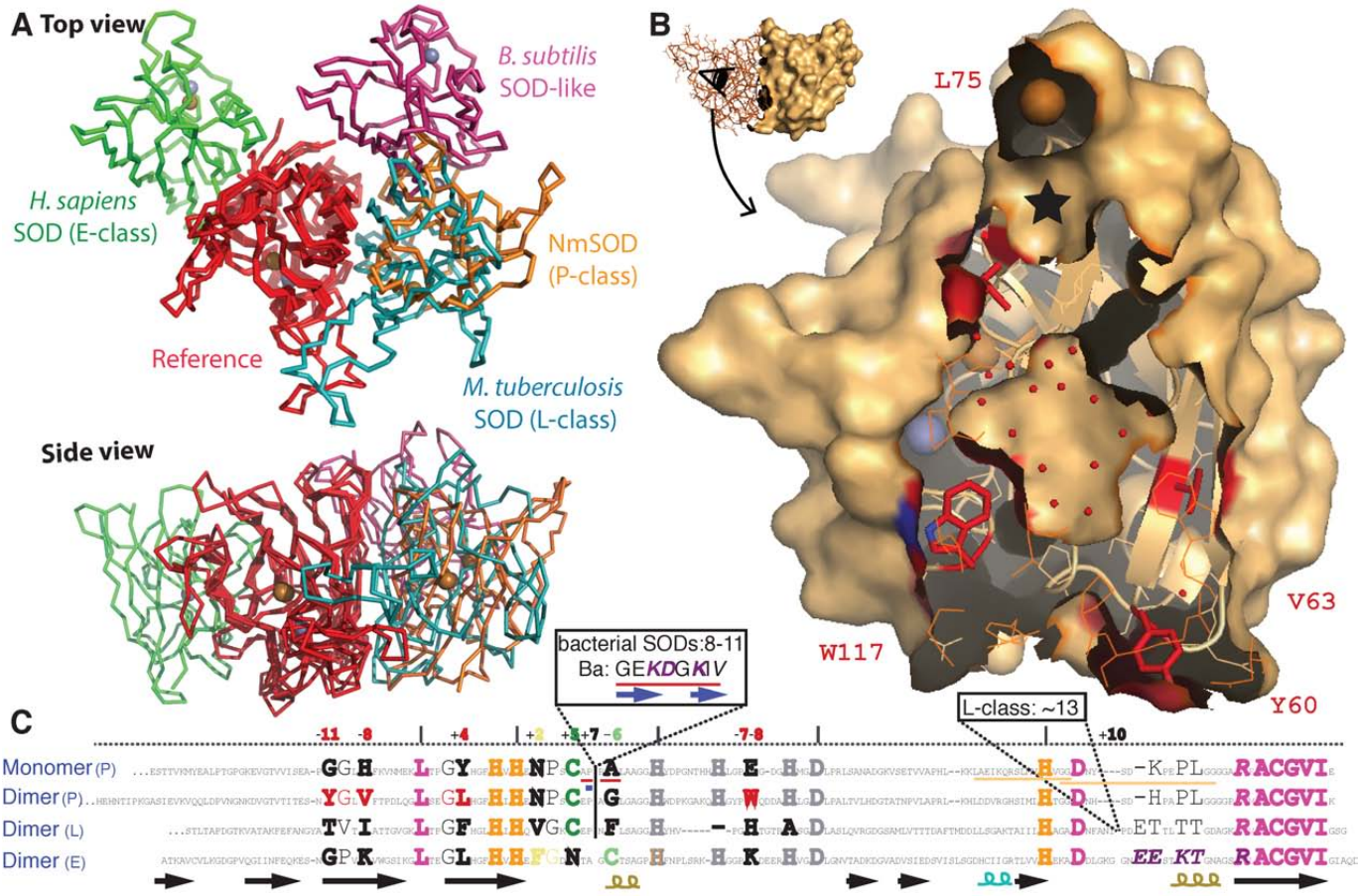
Journal of Bacteriology

JB

Journal of Bacteriology



Accepted Manuscript Posted Online

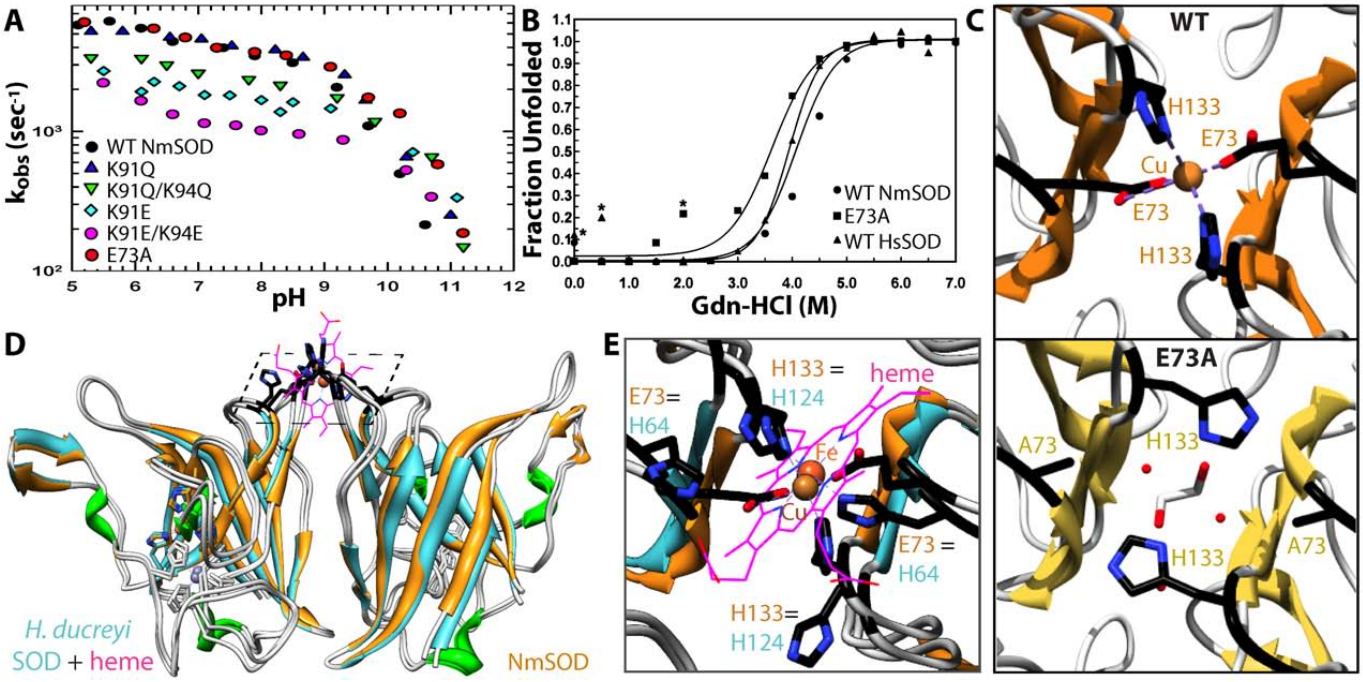


Journal of Bacteriology

JB

Journal of Bacteriology

Accepted Manuscript Posted Online
Journal of Bacteriology
JB
Journal of Bacteriology

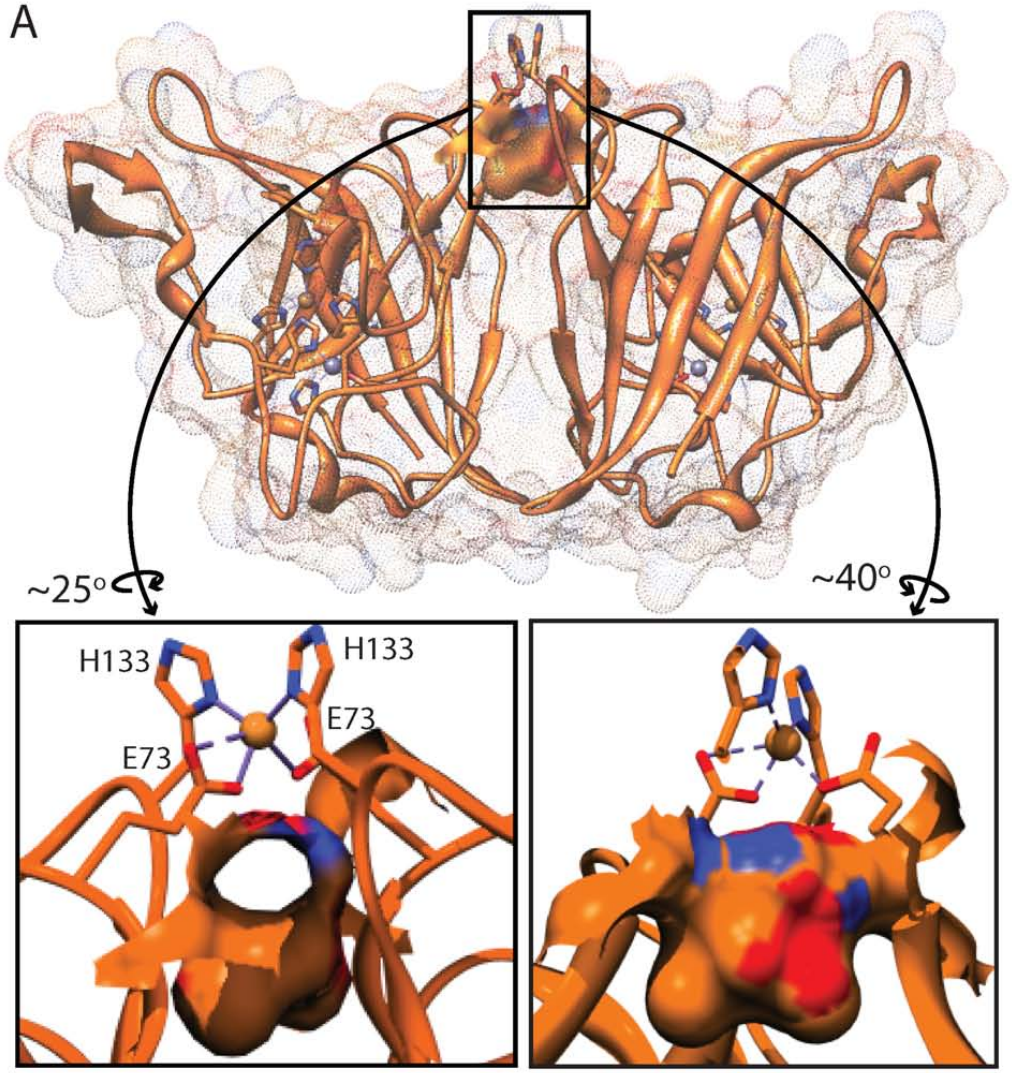


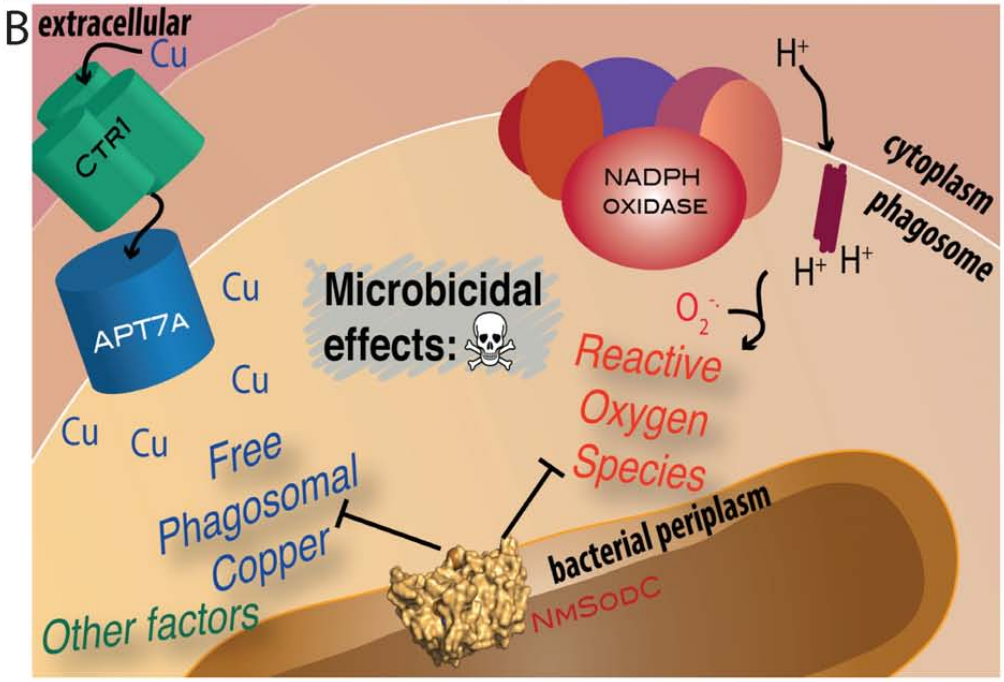
Accepted Manuscript Posted Online

Journal of Bacteriology

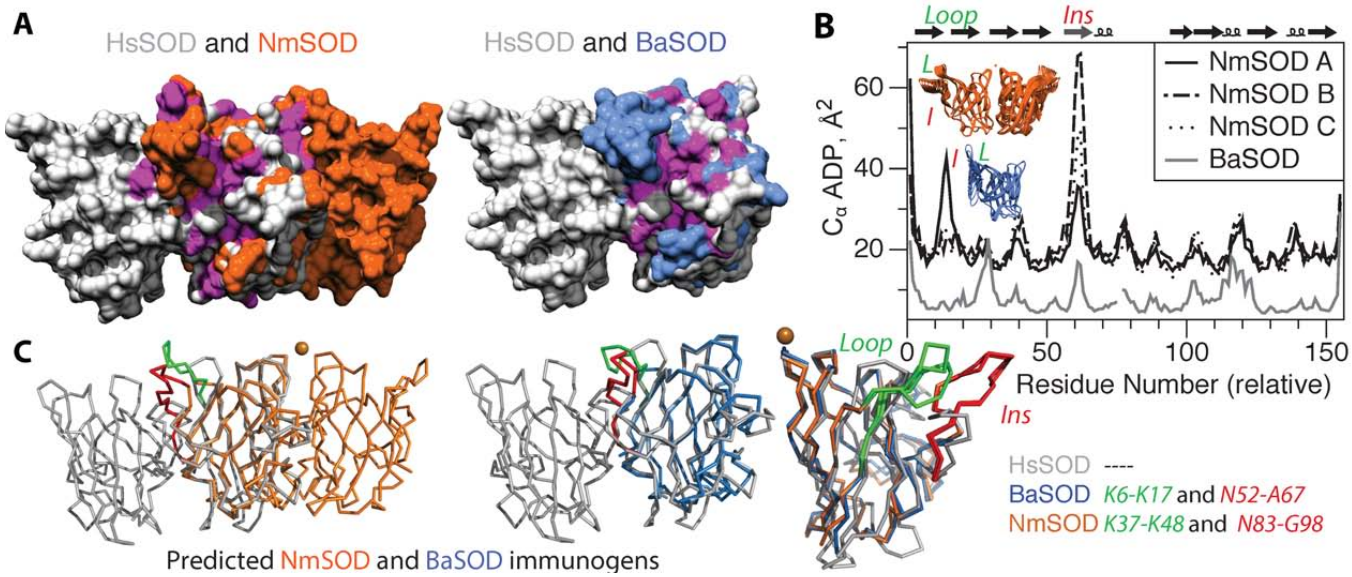
JB

Journal of Bacteriology





Accepted Manuscript Posted Online



Journal of Bacteriology
JB
Journal of Bacteriology